Nexus Science Review
INTERNATIONAL JOURNAL OF INTERDISCIPLINARY RESEARCH

Received: 01/08/2026 - **Accepted:** 13/09/2026
Vol: 01.04
DOI: 10.66104/ypw4n767
Pages: 1-45

Selective Sulfation Roasting and Water Leaching of a Ferruginous Nickel Laterite Using ~0.20 t/t Recorded Commercial H_2SO_4 Solution: Particle-Size-Fraction Response, Iron Rejection, and Process-Value Screening

Antonio Clareti Pereira, PhD
PhD in Chemical Engineering
Federal University of Minas Gerais (UFMG))
Belo Horizonte, Minas Gerais, Brazil
E-mail: claretipereira@gmail.com
ORCID: https://orcid.org/0000-0001-8115-4279

Abstract

Selective sulfation followed by hot-water leaching was evaluated as a screening route for nickel and cobalt recovery from a ferruginous, limonitic laterite using approximately 0.20 t of recorded commercial H_2SO_4 solution per tonne of ore while limiting iron dissolution. This retrospective, archived, single-test screening study reanalyzes six conditions combining two particle-size fractions (<200 mesh and <0.5 mm) with thermal conditioning at 550, 600, and 650 °C. The tests used approximately 197–206 kg of recorded commercial H_2SO_4 solution per tonne of ore; because the acid assay was not preserved, these values are reagent-solution masses rather than 100% H_2SO_4-equivalent dosages. After sulfation at 250 °C for 2 h and thermal conditioning for 4 h, the calcines were leached with water at 90–95 °C for 360 min. Solution-based extraction was calculated from combined pregnant-leach-solution and wash-liquor inventories using the original ore mass. Ni extraction ranged from 68.0 to 88.7%, calculated Co extraction from 81.4 to 94.0%, and Fe dissolution from 7.4 to 19.2%. Co mass-balance closure exceeded 100% across all tests, so small differences in calculated Co extraction should be interpreted with caution and do not support condition-level Co optimization. Within each particle-size fraction, 650 °C gave the strongest observed Ni/Fe response among the tested temperatures; this is a descriptive trend, not a statistical optimum. Complementary mineralogical observations from a separate $FeSO_4 \cdot 7H_2O$ campaign and archived standard-state thermodynamic data support only a working hypothesis involving ferruginous-host dehydroxylation, sulfate transfer from Fe- and Al-bearing sulfates, and possible short-range SO_3 transport. No direct XRD, SEM–EDS, sulfur mapping, or Fe oxidation-state analysis of the present H_2SO_4-based calcines or residues was available, and no gas-speciation proof is claimed. An illustrative process-value screening yielded prethermal indices of approximately US$72–88/t ore before unmeasured thermal energy, off-gas treatment, thermal O&M, and capital costs. The separate atmospheric-leaching dataset is used only as a contextual benchmark because the ores and archived acid-addition bases differ. Because the conditions were not replicated, Test 2 has an estimated mass basis, and classification also altered feed composition, conclusions are limited to descriptive, fraction-specific trends and engineering screening.

Nexus Science Review
INTERNATIONAL JOURNAL OF INTERDISCIPLINARY RESEARCH

Received: 01/08/2026 - **Accepted:** 13/09/2026
Vol: 01.04
DOI: 10.66104/ypw4n767
Pages: 1-45

Further development requires replicated tests, direct characterization of calcine and residue, active-acid normalization, sulfur and energy balances, off-gas measurements, and continuous operability testing.

Keywords: nickel laterite; selective sulfation; sulfation roasting; water leaching; iron rejection; process-value screening.

Highlights

- Approximately 197–206 kg recorded commercial H_2SO_4 solution/t ore yielded 68.0–88.7% Ni extraction with 7.4–19.2% Fe dissolution; the active-acid assay was not preserved.
- Among the tested temperatures, 650 °C gave the strongest observed Ni/Fe response within each particle-size fraction; no statistical optimum is claimed.
- Cross-fraction responses are interpreted as fraction-specific because classification changed both particle size and feed composition, and the tests were not replicated.
- Sulfate-transfer and SO_3-transport mechanisms remain working hypotheses; the process-value indices are illustrative engineering screening, not feasibility results.

Graphical abstract

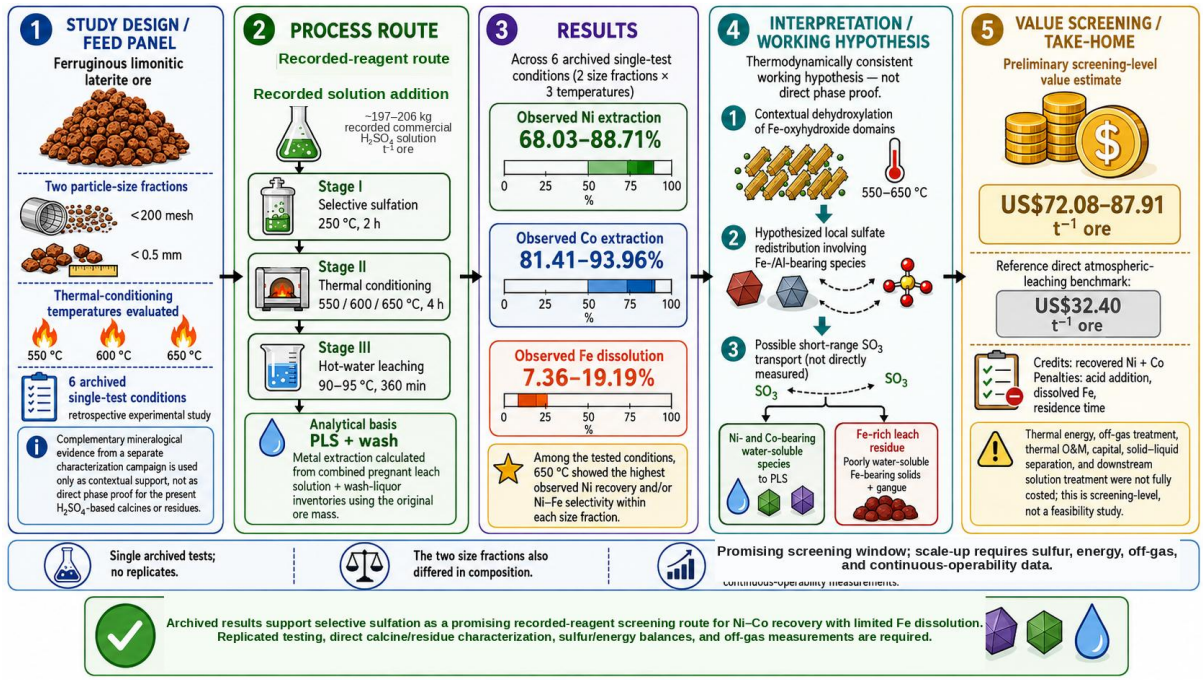

1. Introduction

Nickel laterites are central to the long-term supply of nickel and cobalt because they contain large metal inventories but exhibit unusually heterogeneous mineralogy, variable gangue reactivity, and strong process-route dependence. Recent literature emphasizes that low-

Nexus Science Review
INTERNATIONAL JOURNAL OF INTERDISCIPLINARY RESEARCH

Received: 01/08/2026 - **Accepted:** 13/09/2026
Vol: 01.04
DOI: 10.66104/ypw4n767
Pages: 1-45

grade and mineralogically complex laterites cannot be treated as a single ore class: metal deportment, Fe/Mg/Si distribution, liberation, and the stability of secondary phases jointly control the response to beneficiation, thermal pretreatment, and hydrometallurgical extraction (Acquah et al., 2026; Chi et al., 2026; Zappala et al., 2024). This heterogeneity is particularly important for ferruginous limonitic ores, in which Ni may be structurally incorporated in Fe oxyhydroxides rather than concentrated in a discrete, readily separable mineral. Foundational treatments likewise emphasize that laterite mineralogy and metal deportment must be linked explicitly to process-route selection (Crundwell et al., 2011).

Thermal transformation of the ferruginous host can therefore be as important as reagent chemistry. Goethite dehydroxylation, hematite formation, ferrite transformation, and pretreatment-induced liberation can modify porosity, coordination environment, and accessibility of Ni-bearing domains. Research on limonite dehydroxylation and high-temperature upgrading, together with work on pretreatment-assisted liberation, indicates that the thermal history of the ore should be interpreted as a mineralogical transformation rather than merely as a heating step (Febriana et al., 2024; Gao et al., 2021; Li, Zhu, et al., 2023; Pereira, 2025). Particle-size distribution adds another layer because grinding changes surface area and diffusion length but may also change the proportions of mineral domains reporting to each size fraction (Pereira, 2026).

Conventional atmospheric sulfuric-acid leaching offers relatively simple equipment and avoids high-pressure autoclaves, but ferruginous laterites can require high reagent additions and generate impurity-rich liquors. Dissolved Fe increases neutralization demand, reagent consumption, residue production, and the risk of valuable-metal losses during downstream purification. Iron removal is itself a major hydrometallurgical task, as illustrated by studies of goethite precipitation from laterite-type leach solutions (Das & Li, 2023). The process-design problem is therefore not simply to maximize Ni dissolution, but to maximize valuable Ni–Co recovery while minimizing acid demand, energy use, and downstream impurity burden. This trade-off has long been recognized in atmospheric laterite leaching, where acid consumption, Ni recovery, and soluble Fe are coupled route-selection variables (McDonald & Whittington, 2008).

Nexus Science Review
INTERNATIONAL JOURNAL OF INTERDISCIPLINARY RESEARCH

Received: 01/08/2026 - **Accepted:** 13/09/2026
Vol: 01.04
DOI: 10.66104/ypw4n767
Pages: 1-45

Sulfation roasting followed by water leaching offers a different separation logic. Reactive constituents are first converted to sulfate-bearing phases, after which selective thermal conditioning can decompose Fe-bearing sulfates to poorly soluble oxides while retaining Ni and Co in water-soluble forms. Modern studies have examined this route across serpentine-rich and limonitic feeds, including the effects of alkali salts, MgO and SiO_2, roasting conditions, water leaching, and downstream solvent extraction (Hariyanto et al., 2023a, 2023b, 2024; Mamyrbayeva et al., 2025; Osali et al., 2026; Ribeiro et al., 2020, 2021; Yang et al., 2022). These studies collectively frame sulfation roasting as a selectivity problem involving competing sulfate formation, decomposition, retention, and loss pathways.

Mechanistically, the route is more complex than a single reaction between NiO and sulfuric acid. Low-temperature sulfation of iron oxides and hydroxides, thermodynamic upgrading with Fe(III) sulfate, and recent work on transformation mechanisms and sulfur recovery all point to a network in which Fe- and Al-bearing sulfates may act as sulfate donors, SO_3 may act as a short-range gaseous transfer species, and Mg- or Ca-bearing sulfates may retain sulfur in phases that do not efficiently transfer it to Ni-bearing sites (Gontijo et al., 2020; Souza et al., 2022; Zhao, Li, & Wang, 2025; Zhao, Li, Wang, & Xing, 2024). Process intensification studies have also explored H_2O_2/surfactant-assisted leaching, Na_2SO_4-mediated sulfur transfer, industrial sulfate-bearing secondary reagents, and selective leaching kinetics, demonstrating that sulfur management is increasingly treated as a process variable rather than a fixed reagent input (Candra et al., 2026; Li, Liu, et al., 2026; Zhao, Li, Wang, & Xing, 2025; Zhao et al., 2026).

Optimization studies further show that the best operating point must balance recovery, selectivity, and process penalties rather than maximize a single metallurgical response. Statistical optimization of selective Ni recovery and integrated flowsheet development for low-grade laterites reinforce the need to connect laboratory extraction results with reagent intensity, impurity loading, and scale-up constraints (Khan et al., 2026; Sun et al., 2026). Accordingly, a condition with slightly lower Ni extraction may still be preferable if it materially reduces Fe dissolution, sulfur losses, gas-treatment duty, or required comminution.

Nexus Science Review
INTERNATIONAL JOURNAL OF INTERDISCIPLINARY RESEARCH

Received: 01/08/2026 - **Accepted:** 13/09/2026
Vol: 01.04
DOI: 10.66104/ypw4n767
Pages: 1-45

The present contribution does not claim novelty for sulfation roasting or water leaching themselves. Its specific contribution is the integrated evaluation of a recorded commercial H_2SO_4-solution addition of approximately 0.20 t/t ore, fraction-specific Ni–Co/Fe response on an original-ore inventory basis, impurity dissolution, mass-balance quality, sulfate-transfer plausibility, and an explicitly bounded process-value screening. Recent studies have emphasized optimization, additives, sulfur transfer, and downstream integration (Khan et al., 2026; Osali et al., 2026; Zhao, Li, & Wang, 2025; Zhao, Li, Wang, & Xing, 2024; Zhao et al., 2026). The present archived dataset is therefore positioned as complementary evidence for recorded-reagent selective sulfation rather than as a statistically optimized process, direct mechanistic proof, or final feasibility assessment.

This study examines an archived experimental matrix in which two particle-size fractions of the same ferruginous limonitic ore were subjected to identical nominal sulfation, thermal conditioning, and hot-water leaching procedures at 550, 600, and 650 °C. The objectives were to: (i) describe within-fraction temperature responses for Ni, Co, and Fe without inferential statistical claims; (ii) interpret final pH and Eh states under operational addition of the sulfurous-acid reagent recorded in the historical bulletins as “6 wt.% H_2SO_3”; (iii) integrate complementary mineralogical context with archived standard-state sulfate-transfer thermodynamics while clearly separating indirect evidence from direct measurements; (iv) assess minor-element extraction, filtration, and mass-balance quality; (v) evaluate recovered Ni and Co against recorded acid-reagent addition, dissolved Fe, residence time, and unmeasured thermal/gas-treatment penalties using an illustrative process-value screening index; and (vi) compare the selective-sulfation route with a separate direct atmospheric sulfuric-acid-leaching dataset on an explicitly contextual, non-causal basis. The work is positioned as a retrospective experimental screening study and technology-maturity assessment, not as a replicated optimization study or final feasibility analysis. The evidentiary boundary is fixed by the archive: no condition was replicated; Test 2 uses an estimated mass basis; the active H_2SO_4 assay, direct characterization of the present calcines and residues, sulfur/off-gas balance, and measured furnace energy are unavailable. The article therefore organizes the evidence through an author-developed Recorded-Reagent Selective Sulfation

Nexus Science Review
INTERNATIONAL JOURNAL OF INTERDISCIPLINARY RESEARCH

Received: 01/08/2026 - **Accepted:** 13/09/2026
Vol: 01.04
DOI: 10.66104/ypw4n767
Pages: 1-45

Screening Framework for Ferruginous Laterites (RRSS-FL), which separates direct measurements, derived inventory calculations, complementary mineralogical context, thermodynamic plausibility, process-value screening, and scale-up data gaps.

2. Materials and methods

2.1. Ore samples and particle-size fractions

A ferruginous limonitic nickel laterite was homogenized and divided into two particle-size fractions: a fine fraction passing 200 mesh and a broader fraction below 0.5 mm. Deposit name and site-specific identifiers are intentionally omitted. The two fractions were analyzed separately because classification changed both particle size and chemical composition. The comparison is therefore treated throughout as a particle-size-fraction response rather than as a strictly isolated grinding-size effect. Differences between fractions may reflect size, liberation, mineral-domain partitioning, and composition simultaneously; causal attribution to surface area or diffusion length alone is not made (Pereira, 2026).

Table 1 presents the head grades used in the metal-inventory calculations. The <0.5 mm fraction contained more Ni, Co, and Fe than the <200 mesh fraction, whereas the fine fraction contained more Si and slightly more Mg. Consequently, percentage extraction alone does not fully describe process performance; recovered metal mass per tonne of ore was also calculated.

Table 1. Chemical composition of the two ferruginous laterite particle-size fractions. [Evidence class: direct archived analytical data.]

Component	<200 mesh (wt.%)	<0.5 mm (wt.%)	Process relevance
Al	0.492	0.542	Acid-consuming gangue; potential sulfate donor after $Al_2(SO_4)_3$ formation
Ca	<0.065	<0.065	Potential formation of stable $CaSO_4$
Co	0.099	0.115	Revenue metal
Cr	0.937	0.820	Predominantly refractory impurity associated with chromite
Cu	<0.010	<0.010	Minor impurity
Fe	22.4	28.7	Dominant matrix element and principal impurity penalty
Mg	0.446	0.384	Acid consumer and potential $MgSO_4$ sulfate sink
Mn	0.676	0.853	Reactive impurity; possible Co association
Ni	0.579	0.697	Primary revenue metal
Loss on ignition	4.96	6.20	Structural water and volatile components
Si	27.3	21.8	Quartz/chalcedony and siliceous ferruginous phases
Zn	0.024	0.029	Minor soluble impurity

Nexus Science Review
INTERNATIONAL JOURNAL OF INTERDISCIPLINARY RESEARCH

Received: 01/08/2026 - **Accepted:** 13/09/2026
Vol: 01.04
DOI: 10.66104/ypw4n767
Pages: 1-45

Source: Authors' compilation from archived analytical certificates (Archived Laboratory Campaign, 2011).
Note: Values for the <0.5 mm fraction are duplicate averages, rounded to 3 decimal places. The unrounded Ni grade was retained internally for calculations, but values are reported to the analytical precision appropriate for the archived dataset.

The grade difference has a direct process-value implication. Although the broader fraction generally yielded lower Ni extraction percentages, its higher Ni and Co inventories partly offset that loss. The experimental interpretation therefore distinguishes three responses: extraction percentage, impurity dissolution, and recovered valuable-metal mass.

2.2. Complementary mineralogical characterization

A complementary mineralogical campaign was used to provide context on the likely Ni host and thermal transformation behavior within the broader ore domain. In that campaign, a representative limonitic sample from the same broader ore domain was ground to 100% below 150 µm, mixed with $FeSO_4 \cdot 7H_2O$, treated in a vertical furnace under humid-air injection at 300, 400, or 600 °C for 6 h, and dissolved in deionized water at 90–95 °C for 4 h. Polished centrifuged sections were examined by optical microscopy and SEM–EDS, with X-ray diffraction and bulk chemical analysis used as supporting techniques (Archived Mineralogical Characterization Report, 2009). Because the sulfate reagent, size preparation, atmosphere, and thermal profile differed from the present campaign, these observations are treated only as complementary evidence from the same ore domain and not as direct phase characterization of the H_2SO_4-based calcines or leach residues evaluated here.

Table 2 summarizes the modal results. Within the complementary campaign, Fe oxyhydroxides, grouped as goethite plus hematite due to analytical limitations, accounted for at least 85 wt.% of the solids and were the only identified Ni-bearing phases. Ferrous sulfate was detected in sulfated products but not after water dissolution. These observations establish what occurred in the complementary $FeSO_4 \cdot 7H_2O$ campaign; they are used below only to formulate mechanistic hypotheses for the present H_2SO_4-based tests.

Table 2. Modal mineral composition in the complementary sulfation–dissolution campaign. [Evidence class: complementary mineralogical evidence from a separate campaign.]

Mineral phase	Initial	300 °C sulf.	300 °C diss.	400 °C sulf.	400 °C diss.	600 °C sulf.	600 °C diss.
Quartz/chalcedony	7	6	7	7	6	6	7
K-feldspar	r	r	r	r	r	r	r

Nexus Science Review
INTERNATIONAL JOURNAL OF INTERDISCIPLINARY RESEARCH

Received: 01/08/2026 - **Accepted:** 13/09/2026
Vol: 01.04
DOI: 10.66104/ypw4n767
Pages: 1-45

Biotite	r	r	r	r	r	r	r
Fe oxyhydroxides	92	88	91	86	91	85	90
Ferrous sulfate	–	4	–	7	–	7	–
Chromite	t	1	1	r	2	t	2
Hollandite	t	t	r	t	1	t	t
Asbolane	r	–	–	–	–	–	–

Source: Adapted from the Archived Mineralogical Characterization Report (2009).
Note: Values are wt.%. r < 0.5%; 0.5% < t < 1%. "sulf." = sulfated product; "diss." = residue after water dissolution.

The mineralogical report also recorded a progressive decrease in goethite reflections and a corresponding increase in hematite with increasing treatment temperature, together with more X-ray-amorphous material. This qualitative evolution is consistent with the broader literature on goethite-to-hematite transformation and limonite dehydroxylation (Li, Zhu, et al., 2023; Pereira, 2025).

Figure 1 summarizes the three-stage process concept used in the present campaign. The sequence separates low-temperature sulfation from high-temperature selective conditioning and then uses hot water to dissolve the soluble sulfate inventory.

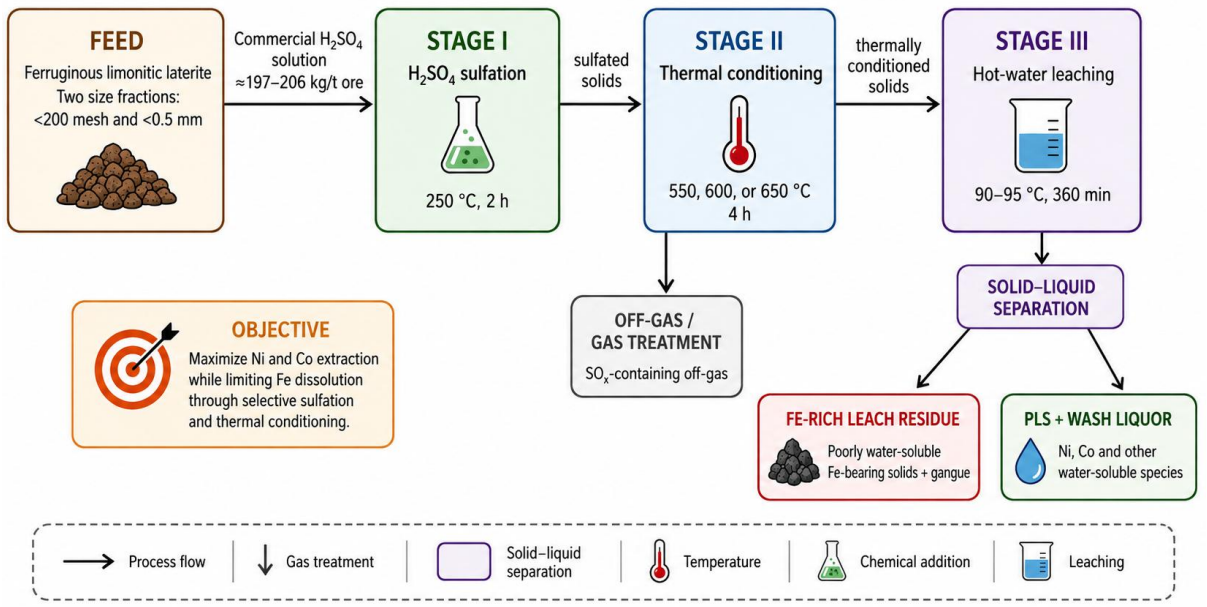

Figure 1. Conceptual flowsheet for selective sulfation, thermal conditioning, and hot-water leaching of the ferruginous nickel laterite. [Evidence class: author-developed process concept based on the archived procedure.]
Source: Authors' conceptual synthesis from the archived experimental procedure (Archived Laboratory Campaign, 2011).

Nexus Science Review
INTERNATIONAL JOURNAL OF INTERDISCIPLINARY RESEARCH

Received: 01/08/2026 - **Accepted:** 13/09/2026
Vol: 01.04
DOI: 10.66104/ypw4n767
Pages: 1-45

The flowsheet highlights a central process feature: sulfur is redistributed rather than simply consumed. Sulfur can remain in valuable-metal sulfates, persist in Fe- or gangue-bearing sulfates, or leave with SO_x-containing off-gas. The metallurgical optimum therefore depends on both solid-state phase transformation and sulfur retention in the reaction zone.

2.3. Experimental matrix

The present campaign comprised six conditions generated by combining two particle-size fractions with three thermal-conditioning temperatures. All tests used the same nominal sulfation reagent ratio and the same water-leaching duration. Table 3 summarizes the matrix.

Nexus Science Review
INTERNATIONAL JOURNAL OF INTERDISCIPLINARY RESEARCH

Received: 01/08/2026 - **Accepted:** 13/09/2026
Vol: 01.04
DOI: 10.66104/ypw4n767
Pages: 1-45

Table 3. Experimental matrix for the selective-sulfation campaign. [Evidence class: direct archived experimental design records.]

Test	Particle-size fraction	Ore (nominal g)	H_2O in sulfation (g)	Acid (g)	Sulfation	Conditioning	Water leach
1	<200 mesh	400	20	80	250 °C, 2 h	650 °C, 4 h	1000 g H_2O; 90–95 °C; 6 h
2	<200 mesh	400	20	80	250 °C, 2 h	600 °C, 4 h	1000 g H_2O; 90–95 °C; 6 h
3	<200 mesh	400	20	80	250 °C, 2 h	550 °C, 4 h	1000 g H_2O; 90–95 °C; 6 h
7	<0.5 mm	400	20	80	250 °C, 2 h	650 °C, 4 h	1000 g H_2O; 90–95 °C; 6 h
8	<0.5 mm	400	20	80	250 °C, 2 h	600 °C, 4 h	1000 g H_2O; 90–95 °C; 6 h
9	<0.5 mm	400	20	80	250 °C, 2 h	550 °C, 4 h	1000 g H_2O; 90–95 °C; 6 h

Source: Authors' compilation from the archived work plan and operating bulletins (Archived Laboratory Campaign, 2011).
Note: Actual ore and combined reagent masses varied slightly around the nominal values. "Acid solution" denotes the recorded commercial H_2SO_4 solution used in the archived campaign.

The matrix permits a descriptive within-fraction assessment of conditioning temperature. Cross-fraction comparisons are informative but combine particle size and feed-composition effects; they are therefore interpreted as practical fraction responses rather than as a pure comminution experiment. Because each condition was run once, differences are reported as observed trends and are not assigned statistical significance.

2.4. Sulfation and thermal conditioning

Ore was mixed with water and the recorded commercial sulfuric-acid solution, and the resulting material was placed in a muffle furnace. The first stage was maintained near 250 °C for 2 h to promote dehydration and initial sulfate formation. The furnace temperature was then increased to 550, 600, or 650 °C and maintained for 4 h. No controlled bulk gas flow was recorded for the present muffle-furnace tests; the atmosphere was nominally air, while local O_2 and SO_x partial pressures within the static bed were not measured.

Nexus Science Review
INTERNATIONAL JOURNAL OF INTERDISCIPLINARY RESEARCH

Received: 01/08/2026 - **Accepted:** 13/09/2026
Vol: 01.04
DOI: 10.66104/ypw4n767
Pages: 1-45

Table 4 reports actual mass data and estimated commercial-acid dosages. The acid dosage was calculated by assuming that the recorded combined reagent mass preserved the nominal 80:20 mass ratio of commercial H_2SO_4 solution to added water. This assumption is explicit because the historical sulfation bulletin reported only the combined reagent mass. The assay or purity of the commercial acid was not preserved in the surviving records; consequently, all acid dosages in the selective-sulfation campaign are reported on a commercial-acid-solution mass basis and should not be interpreted as 100% H_2SO_4-equivalent additions.

Table 4. Sulfation mass data, estimated acid dosage, and thermal mass loss. [Evidence class: direct archived mass data with derived reagent-solution calculations.]

Test	Fraction	T (°C)	Ore mass (g)	Combined reagent (g)	Calcine/ product (g)	Mass loss (%)	Estimated commercial H_2SO_4 solution addition (kg/t ore)
1	<200 mesh	650	387.13	99.82	407.58	16.30	206.28
2	<200 mesh	600	400.00*	100.00*	435.91	n.a.	200.00*
3	<200 mesh	550	397.32	100.09	438.77	11.79	201.53
7	<0.5 mm	650	402.62	99.75	420.80	16.24	198.20
8	<0.5 mm	600	405.15	99.93	437.32	13.42	197.32
9	<0.5 mm	550	407.09	100.24	441.77	12.92	196.99

Source: Authors' calculations from archived sulfation operating bulletins (Archived Laboratory Campaign, 2011).
Note: *The original sulfation bulletin for Test 2 was not recovered. The nominal 400 g ore and 80 g commercial H_2SO_4-solution values were therefore used. "n.a." = not available.

For both fractions, the highest observed mass loss occurred at 650 °C. Mass loss is consistent with dehydration, goethite dehydroxylation, decomposition of Fe-bearing sulfates, and release of H_2O and sulfur-bearing gases, but it cannot by itself distinguish productive sulfate transfer from undesirable sulfur loss.

2.5. Hot-water leaching and redox control

After thermal conditioning, calcined products were leached with approximately 1000 g of water at 90–95 °C for 360 min under agitation. Pulp pH and Eh were recorded. A reducing reagent designated in the archived operating bulletins as "6 wt.% H_2SO_3 solution" was added

Nexus Science Review
INTERNATIONAL JOURNAL OF INTERDISCIPLINARY RESEARCH

Received: 01/08/2026 - **Accepted:** 13/09/2026
Vol: 01.04
DOI: 10.66104/ypw4n767
Pages: 1-45

at selected times to lower the measured redox potential. This historical designation is retained for traceability; aqueous $SO_2/H_2SO_3/HSO_3^-$ speciation was not independently reconstructed. The reference electrode used for the historical Eh measurements was not preserved in the records; therefore, Eh values are reported as instrument readings in millivolts and are not converted to the standard hydrogen electrode scale.

Table 5 reports the principal operating and final-solution data. PLS analytical samples were diluted fivefold before analysis, whereas wash-liquor values were used as reported. PLS and wash volumes were calculated from measured mass and density.

Table 5. Water-leaching operation, final pH/Eh, and solid–liquid separation data. [Evidence class: direct archived operating and final-solution data.]

Test	Calcine leached (g)	PLS volume (mL)	Wash volume (mL)	Dry residue (g)	H_2SO_3 6% (mL)	Reactor pH at 360 min	Reactor Eh at 360 min (mV)	PLS pH	PLS Eh (mV)	Time
1	407.57	733.70	1876.86	347.36	10.36	1.30	579.0	1.17	519.5	5:24
2	435.91	770.01	1880.14	347.12	25.90	1.12	588.5	1.09	516.8	12:33
3	437.17	792.48	1865.59	343.62	31.08	1.11	588.7	1.07	521.2	12:25
7	420.80	720.16	1887.73	357.72	20.72	1.23	589.0	1.10	508.1	11:06
8	435.54	755.89	1877.79	350.97	31.08	0.70	586.0	0.73	516.0	10:17
9	440.91	756.91	1877.63	351.92	20.72	1.10	600.8	1.06	548.4	12:50

Source: Authors' compilation from archived leaching operating bulletins (Archived Laboratory Campaign, 2011). Test 2 is retained for descriptive screening; its original sulfation mass bulletin was not recovered.
Note: Filtration time is the sum of PLS and wash filtration times. Eh values are uncorrected instrument readings because the reference electrode was not documented. "6 wt.% H_2SO_3" is the archived reagent designation; aqueous sulfurous-acid speciation was not independently reconstructed.

Because addition of the archived "6 wt.% H_2SO_3" reagent differed among tests, Eh was an operationally controlled response rather than an independent experimental factor. The reagent can also affect acidity and Fe(III)/Fe(II) speciation; therefore, dose is treated as a potential confounder rather than as a mechanistically isolated variable. The pH and Eh data are used descriptively, and extraction differences are not attributed to redox potential or reductant addition alone.

2.6. Chemical analysis and extraction calculation

PLS, wash liquor, feed, and dry residues were analyzed for major and minor elements using the analytical results preserved in the archived certificates and operating records. Solution-based extraction was selected as the primary response because it directly measures

Nexus Science Review
INTERNATIONAL JOURNAL OF INTERDISCIPLINARY RESEARCH

Received: 01/08/2026 - **Accepted:** 13/09/2026
Vol: 01.04
DOI: 10.66104/ypw4n767
Pages: 1-45

the dissolved inventory and includes metal recovered in the wash step. For the PLS, reported concentration was multiplied by the fivefold dilution factor. The surviving archive does not preserve a complete instrumental QA/QC dossier, including the instrument model, calibration curves, certified reference material results, or LOD/LOQ values. Accordingly, the manuscript does not assign a formal analytical uncertainty that cannot be reconstructed; mass-balance closure is instead used as an empirical data-quality diagnostic, and no analytical result was adjusted to enforce closure.

$$V_l = m_l / (\rho_l \times 1000) \quad (1)$$

$$Vw = mw / (\rho w \times 1000) \quad (2)$$

$$m_i,diss = C_{i,l}\, f\, V_l + C_{i,w}\, Vw \quad (3)$$

$$m_i,0 = m_{ore}\, (G_i/100) \quad (4)$$

$$X_i = 100 \times m_i,diss / m_i,0 \quad (5)$$

In Eqs. (1)–(5), V is liquid volume, m is liquid or ore mass, ρ is liquid density, C is analytical concentration, f is the PLS dilution factor, G_i is the head grade of element i, and X_i is solution-based extraction or dissolution. For Ni and Co, X_i represents recovery to solution; for Fe and other gangue elements, it represents the dissolution of impurities.

The original ore mass was used instead of calcine mass. This correction is essential because applying feed-grade to the calcine mass would overstate the original metal inventory after sulfur addition and volatile loss. Original ore masses were recovered for Tests 1, 3, and 7–9; Test 2 uses the nominal 400 g ore mass and is flagged as estimated.

2.7. Selectivity, thermodynamic, and process-value indicators

Two selectivity indicators were used. The first compares extraction percentages and is convenient for within-feed comparisons. The second compares the recovered Ni plus Co mass with the dissolved Fe mass and is more directly related to the downstream purification burden.

$$SNi/Fe = XNi / XFe \quad (6)$$

$$Smass = (mNi,rec + mCo,rec) / mFe,diss \quad (7)$$

Thermodynamic reaction data preserved in the archived project dataset were evaluated at 550, 600, and 650 °C. Standard Gibbs energy and equilibrium constants were used only to test whether selected sulfate-transfer reactions were thermodynamically plausible under standard-state assumptions. The original software and thermodynamic-database metadata used

Nexus Science Review
INTERNATIONAL JOURNAL OF INTERDISCIPLINARY RESEARCH

Received: 01/08/2026 - **Accepted:** 13/09/2026
Vol: 01.04
DOI: 10.66104/ypw4n767
Pages: 1-45

to assemble the archived ΔG° values were not preserved; consequently, the analysis is treated as an archived-data consistency screen rather than as a newly generated, independently reproducible equilibrium calculation. The reported log K values were checked for arithmetic consistency with the tabulated ΔG° values. NiO is used as a thermodynamic proxy for a Ni-bearing oxide component and is not claimed to be an experimentally identified discrete phase in the ore. These calculations establish thermodynamic plausibility only; they do not demonstrate reaction rate, phase abundance, gas composition, or the dominant pathway in the heterogeneous ore.

The preliminary process-value screening credits recovered Ni and Co and applies transparent, illustrative penalties for recorded acid-reagent addition, dissolved Fe, and residence time. The coefficients are author-defined screening assumptions used solely for internal comparison; they are not presented as current market forecasts or site-specific operating costs. Thermal energy, off-gas treatment, solids handling, maintenance, and annualized CAPEX were excluded from the prethermal index and treated only as a break-even allowance. The resulting values are comparative engineering indices, not cash-flow forecasts, project economics, NPV, IRR, or feasibility estimates.

$$R_{Ni+Co} = m_{Ni,rec} P_{Ni} + m_{Co,rec} P_{Co} \quad (8)$$

$$I_{prethermal} = R_{Ni+Co} - C_{acid} - C_{Fe} - C_{time} \quad (9)$$

$$I_{final} = I_{prethermal} - C_{energy} - C_{gas} - C_{capital} - C_{thermal,O\&M} \quad (10)$$

2.8. Direct atmospheric-leaching benchmark

Selective-sulfation results were compared with a separate archived dataset of atmospheric sulfuric acid leaching for another ferruginous laterite. That benchmark reported 700–1000 kg H_2SO_4/t ore, 95–100 °C, and residence times of 30–420 min (Archived Atmospheric-Leaching Benchmark Dataset, n.d.). The selective-sulfation values, however, are masses of commercial H_2SO_4 solution for which assay was not preserved. Because the two datasets do not share a demonstrably common active-H_2SO_4 basis, the recorded reagent additions are not interpreted as normalized acid-consumption values. The ores, grades, mineralogy, and experimental programs also differed. Accordingly, the comparison is explicitly a process-context benchmark used to illustrate trade-offs among recorded reagent

Nexus Science Review
INTERNATIONAL JOURNAL OF INTERDISCIPLINARY RESEARCH

Received: 01/08/2026 - **Accepted:** 13/09/2026
Vol: 01.04
DOI: 10.66104/ypw4n767
Pages: 1-45

intensity, Ni–Co recovery, and dissolved Fe, not to claim causal, metallurgical, or economic superiority.

2.9. Scope of inference, analytical uncertainty, and data-quality limitations

The six selective-sulfation conditions were historical single tests rather than replicated experiments designed for formal statistical inference. Accordingly, the manuscript reports observed trends, mass-balance closure, and mechanistic consistency without p values, confidence intervals, ANOVA, or claims of statistical significance. The evidence is interpreted in four levels: (1) direct measurements from the present campaign (mass, solution chemistry, residue assays, pH/Eh, filtration time); (2) derived inventories and closure calculations; (3) complementary mineralogical observations from a separate $FeSO_4 \cdot 7H_2O$ campaign; and (4) archived standard-state thermodynamic plausibility. Conclusions are worded to preserve these distinctions. Co closures above 100% indicate material analytical uncertainty at low feed and residue grades, while the missing original Test 2 sulfation bulletin adds uncertainty because nominal ore/reagent masses are used. The unresolved assay of the commercial acid and the non-normalized acid basis of the separate direct-leach benchmark are additional boundaries on reagent-intensity comparisons. These limitations are intrinsic to the archived dataset and are not treated as if they could be removed by post hoc statistical analysis.

The surviving archive does not permit reconstruction of a formal instrumental measurement-uncertainty budget. Mass-balance closure is therefore used only as an empirical data-quality flag: Ni closure ranged from 98.56 to 110.86%, Co from 107.67 to 115.14%, and Fe from 95.69 to 101.56%. These ranges do not justify post hoc correction of individual extractions. Ni and Fe differences are retained as descriptive screening responses without confidence intervals, whereas the systematic positive Co closure and low Co head grade make small Co differences particularly unreliable; the defensible Co conclusion is substantial recovery across the tested window rather than condition-level optimization. Test 2 uses nominal ore and reagent masses because its original sulfation bulletin was not recovered and is therefore treated as estimated-basis only; it is not used for any unqualified ranking-sensitive conclusion.

Nexus Science Review
INTERNATIONAL JOURNAL OF INTERDISCIPLINARY RESEARCH

Received: 01/08/2026 - **Accepted:** 13/09/2026
Vol: 01.04
DOI: 10.66104/ypw4n767
Pages: 1-45

3. Results and discussion

3.1. Mineralogical basis for selective sulfation

Within the complementary mineralogical campaign, Ni was not concentrated in a discrete mineral. Fe oxyhydroxides represented more than 85 wt.% of the solids and were the only identified Ni carriers in that separate sample set. SEM–EDS indicated approximately 1.3 wt.% Ni in the initial Fe oxyhydroxides, with individual analyses ranging from 0 to 2 wt.%. The same phases contained Cr, Mn, and Mg, confirming chemical heterogeneity of the ferruginous matrix. These observations provide context for the present interpretation but are not direct phase measurements of Tests 1–3 and 7–9.

In the complementary campaign, heating was reported to progressively reduce goethite-related reflections, increase hematite-related reflections, and increase the poorly crystalline or X-ray-amorphous contribution. The principal structural reaction used to interpret that trend is dehydroxylation:

$$2FeOOH \rightarrow Fe_2O_3 + H_2O(g) \quad (11)$$

Dehydroxylation can create pores and microcracks, alter the local coordination of substituted Ni, and expose previously inaccessible reaction sites; excessive recrystallization or sintering, however, can reduce accessibility. This duality is consistent with published work on limonite phase transformation, high-temperature upgrading, and goethite-to-hematite conversion (Gao et al., 2021; Li, Zhu, et al., 2023; Pereira, 2025).

Figure 2 converts the qualitative observations from the complementary campaign into a non-quantitative phase-evolution schematic. It intentionally avoids numerical axes, synthetic intensities, or implied phase fractions and should not be interpreted as measured XRD data for the present H_2SO_4-based calcines.

Nexus Science Review
INTERNATIONAL JOURNAL OF INTERDISCIPLINARY RESEARCH

Received: 01/08/2026 - **Accepted:** 13/09/2026
Vol: 01.04
DOI: 10.66104/ypw4n767
Pages: 1-45

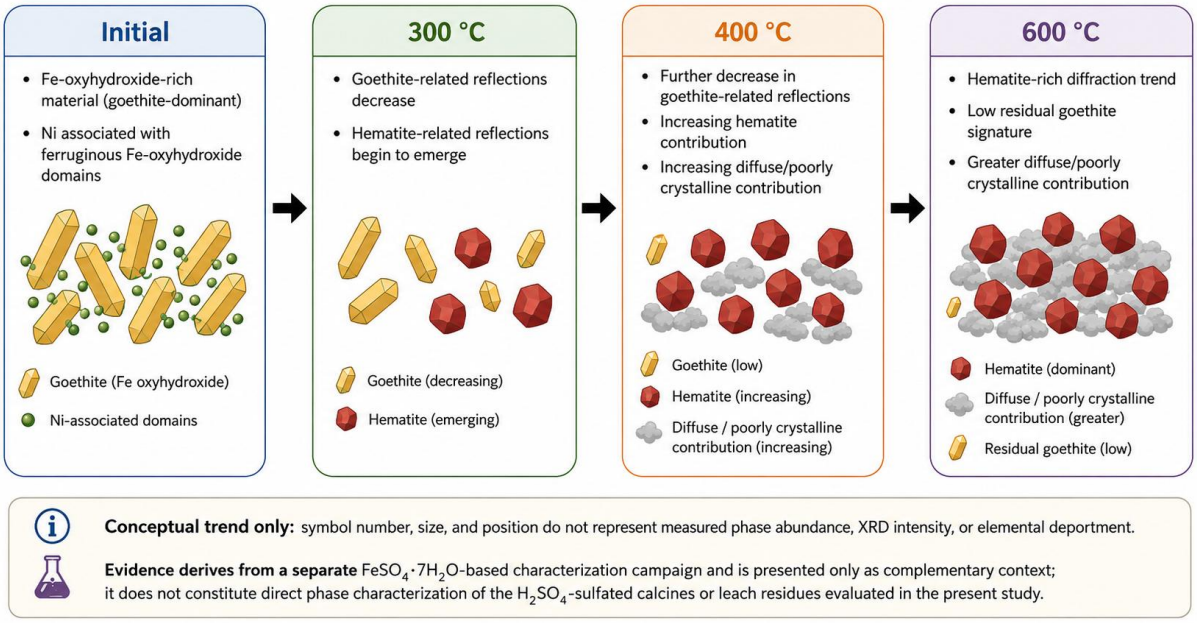

Figure 2. Qualitative phase-evolution concept from the complementary $FeSO_4 \cdot 7H_2O$ sulfation–dissolution campaign; box positions do not represent measured phase abundance or XRD intensity. [Evidence class: author-developed qualitative schematic from complementary evidence.]
Source: Authors' schematic reconstruction from qualitative observations in the Archived Mineralogical Characterization Report (2009); not direct XRD characterization of the present H_2SO_4-based calcines or residues.

The complementary observations make host transformation a plausible component of the thermal response. The present process should therefore not be reduced conceptually to dissolution of pre-existing NiO. Rather, Ni accessibility may evolve as the ferruginous host dehydroxylates, recrystallizes, and interacts with sulfate-bearing species. Because direct phase characterization of the present calcines and residues is unavailable, this interpretation remains mechanistic context rather than phase proof. Pretreatment research on low-grade laterites likewise emphasizes liberation and host transformation as controls on recovery (Febriana et al., 2024).

3.2. Thermal mass loss and sulfate mobility

For the <200 mesh fraction, thermal mass loss increased from 11.79% at 550 °C to 16.30% at 650 °C; the 600 °C value was unavailable. For the <0.5 mm fraction, mass loss increased from 12.92 to 13.42 and 16.24% at 550, 600, and 650 °C, respectively. The nearly

Nexus Science Review
INTERNATIONAL JOURNAL OF INTERDISCIPLINARY RESEARCH

Received: 01/08/2026 - **Accepted:** 13/09/2026
Vol: 01.04
DOI: 10.66104/ypw4n767
Pages: 1-45

identical values at 650 °C are consistent with a strong temperature contribution to bulk volatile release and sulfate decomposition, but they do not isolate a particle-size effect because the classified fractions also differed in composition.

Figure 3 compares thermal mass loss for the two size fractions. The missing Test 2 value is explicitly left unavailable rather than interpolated.

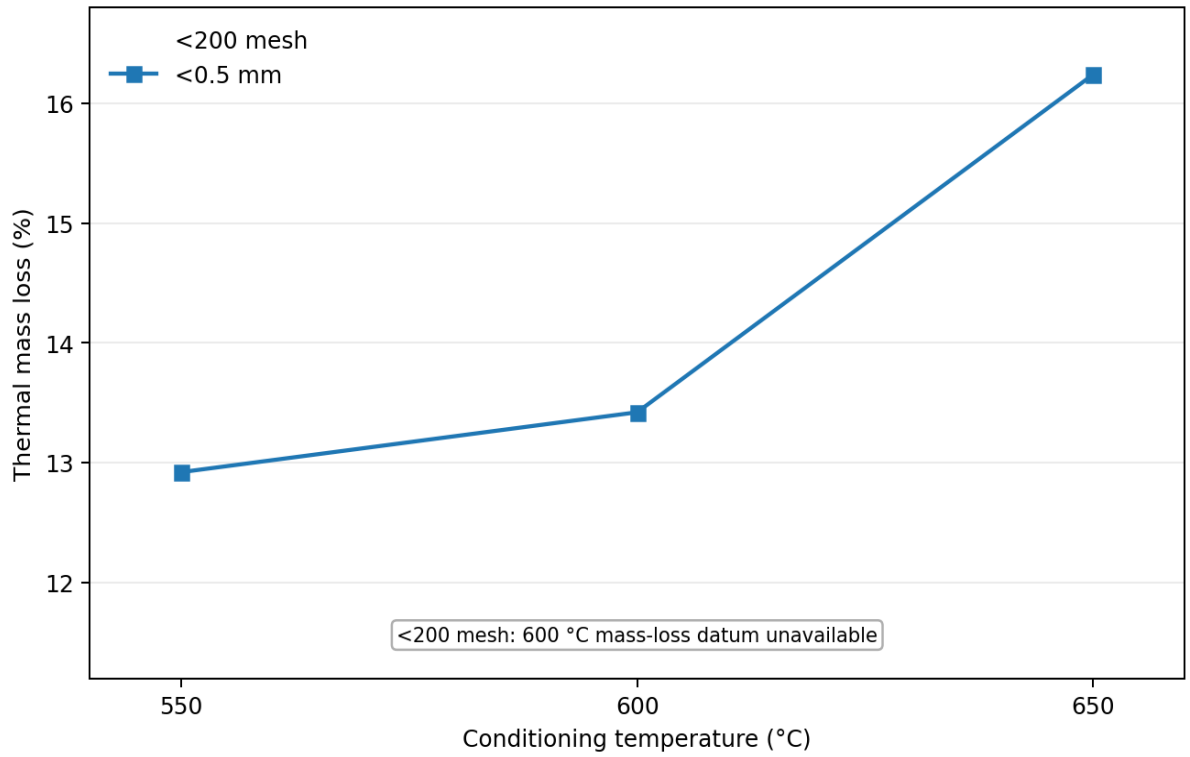

Figure 3. Thermal mass loss as a function of conditioning temperature for the <200 mesh and <0.5 mm fractions. [Evidence class: derived trend from archived mass data.]
Source: Authors' calculations from archived sulfation operating bulletins (Archived Laboratory Campaign, 2011). Note: No mass-loss value was available for the <200 mesh fraction at 600 °C; the missing datum was not interpolated.

Higher mass loss at 650 °C is consistent with, but does not uniquely demonstrate, stronger dehydration, goethite dehydroxylation, and decomposition of Fe-bearing sulfate species. Low-temperature sulfation studies of iron oxides and laterite roasting literature support treating Fe-sulfate stability as a temperature-sensitive control on subsequent Fe dissolution (Gontijo et al., 2020; Ribeiro et al., 2021; Zhao, Li, Wang, & Xing, 2024). The same mass-loss trend also signals potentially greater off-gas duty, making sulfur capture and gas treatment integral scale-up questions.

Nexus Science Review
INTERNATIONAL JOURNAL OF INTERDISCIPLINARY RESEARCH

Received: 01/08/2026 - **Accepted:** 13/09/2026
Vol: 01.04
DOI: 10.66104/ypw4n767
Pages: 1-45

3.3. Final pH and Eh states during water leaching

Corrected initial water pH values were approximately 2.63–2.98. After calcine addition, the liquors became strongly acidic. Final reactor pH ranged from 0.70 to 1.30 and PLS pH from 0.73 to 1.17, showing that the nominal "water-leaching" step actually operated in an acidic environment created by residual acid, soluble sulfates, and hydrolysis reactions. Test 8 gave the lowest final pH, indicating either greater residual acidity or a larger inventory of hydrolysable sulfate species.

Because the archived operating records preserve reliable final-state pH and total addition of the reducing reagent designated as "6 wt.% H_2SO_3," but not a complete time-resolved dataset suitable for replotting, Figure 4 presents only the measured final pH values together with total reagent addition.

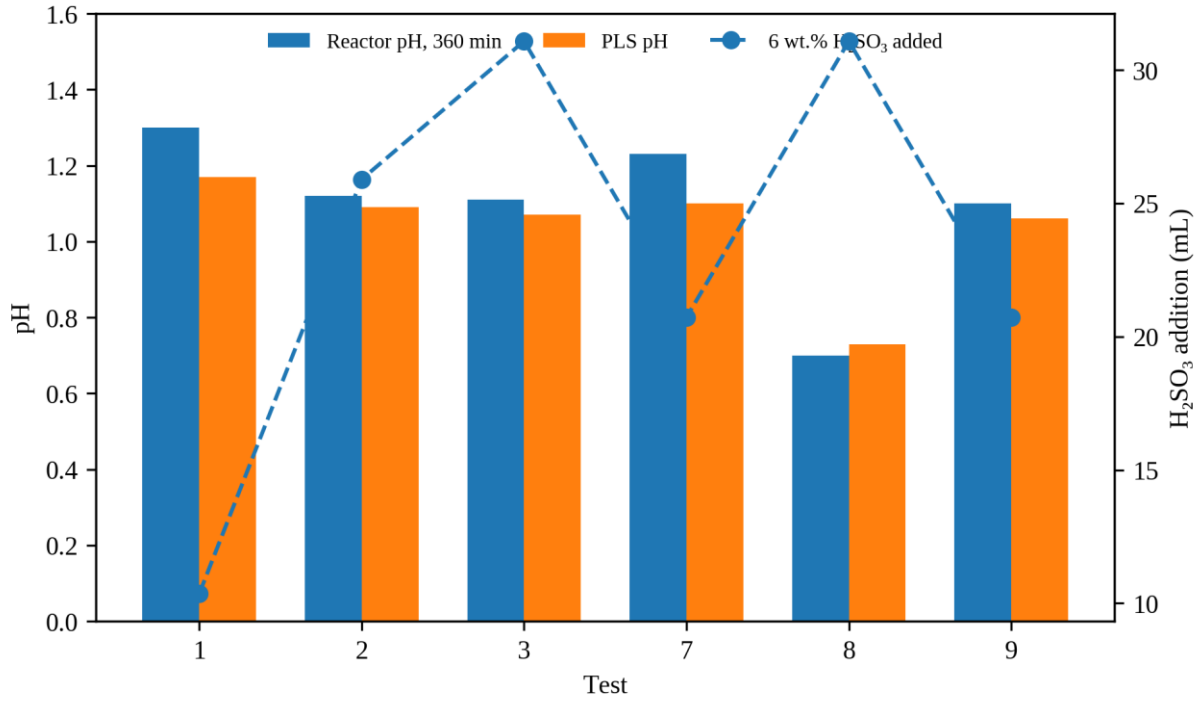

Figure 4. Final reactor and PLS pH values with total addition of the archived "6 wt.% H_2SO_3" reducing reagent for Tests 1–3 and 7–9. [Evidence class: direct archived final-state operating data.]
Source: Authors' compilation from archived leaching operating bulletins (Archived Laboratory Campaign, 2011).

The strongly acidic final state explains why residual Fe sulfates and other soluble gangue phases can contribute to the solution inventory even though the leachant is water. The

Nexus Science Review
INTERNATIONAL JOURNAL OF INTERDISCIPLINARY RESEARCH

Received: 01/08/2026 - **Accepted:** 13/09/2026
Vol: 01.04
DOI: 10.66104/ypw4n767
Pages: 1-45

need to separate the thermal selectivity step from subsequent aqueous impurity management is consistent with the wider hydrometallurgical emphasis on Fe control in laterite liquors (Das & Li, 2023; Chi et al., 2026).

Final reactor Eh readings were 579–601 mV, whereas filtered PLS readings were lower, 508–548 mV. Recorded additions of the "6 wt.% H_2SO_3" reagent ranged from 10.36 to 31.08 mL, confirming that redox conditions were operationally manipulated rather than imposed as a single fixed experimental factor.

Figure 5 therefore compares final Eh measurements with total recorded reducing-reagent addition rather than implying a fully reconstructed time trajectory.

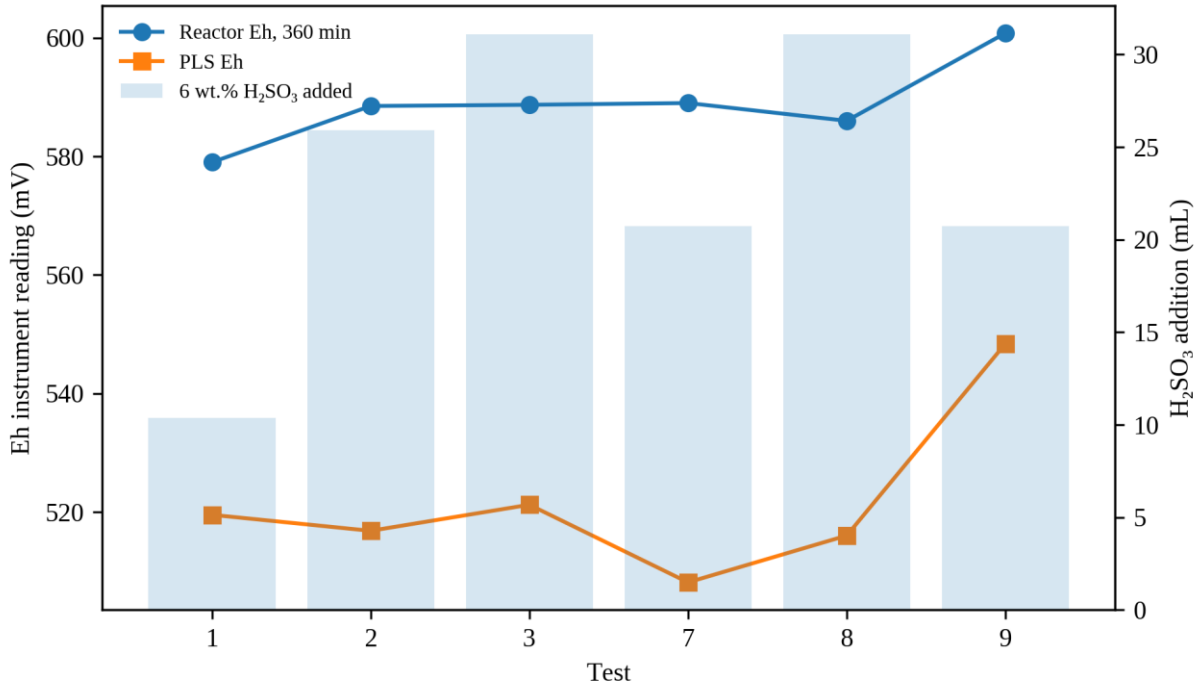

Figure 5. Final reactor and PLS Eh instrument readings with total addition of the archived "6 wt.% H_2SO_3" reducing reagent. [Evidence class: direct archived final-state operating data.]

Source: Authors' compilation from archived leaching operating bulletins (Archived Laboratory Campaign, 2011); Eh values are uncorrected instrument readings. Test 2 is retained for descriptive screening; its original sulfation mass bulletin was not recovered.

The larger reducing-reagent additions in Tests 2, 3, and 8 are compatible with greater reductant demand, but the cause cannot be isolated because dose was operationally adjusted and the reference-electrode basis was not preserved. Fe^{2+} measured in final liquor cannot independently prove that $FeSO_4$ was present in the present calcine because the added reducing

Nexus Science Review
INTERNATIONAL JOURNAL OF INTERDISCIPLINARY RESEARCH

Received: 01/08/2026 - **Accepted:** 13/09/2026
Vol: 01.04
DOI: 10.66104/ypw4n767
Pages: 1-45

reagent can reduce dissolved Fe^{3+}. The redox data are therefore used only as final-state operating descriptors and not as proof of calcine speciation. Future campaigns should document the reference electrode, temperature-corrected Eh basis and conversion to the standard hydrogen electrode scale, time-resolved pH/Eh, Fe^{2+}/Fe^{3+} ratio, sulfite/sulfate speciation, and reducing-reagent consumption.

3.4. Main metal extraction and iron rejection

Table 6 summarizes the principal metallurgical results on the corrected original-ore basis. Test 1, the fine fraction conditioned at 650 °C, gave the highest observed Ni and Co extractions. Test 7, the broader fraction conditioned at 650 °C, gave the lowest observed Fe dissolution and the highest percentage-based Ni/Fe selectivity. These are the best tested responses in the archived matrix; no statistical optimum is claimed.

Table 6. Corrected Ni and Co extraction, Fe dissolution, and selectivity indicators. [Evidence class: derived extraction/selectivity calculations from archived analyses.]

Test	Fraction	T (°C)	Ni extraction (%)	Co extraction (%)	Fe dissolution (%)	Ni/Fe	(Ni+Co)/Fe (g/g)
1	<200 mesh	650	88.71	93.96	9.03	9.82	0.300
2	<200 mesh	600	77.88*	90.40*	17.43*	4.47	0.138
3	<200 mesh	550	76.41	93.19	19.19	3.98	0.124
7	<0.5 mm	650	76.55	81.41	7.36	10.40	0.297
8	<0.5 mm	600	73.68	82.75	12.47	5.91	0.170
9	<0.5 mm	550	68.03	88.43	12.56	5.42	0.160

Source: Authors' calculations from combined PLS and wash-liquor inventories.
Note: *Estimated using the nominal 400 g original ore mass because the Test 2 sulfation bulletin was not recovered.

For the fine fraction, the observed change from 550 to 650 °C corresponded to a 12.30-percentage-point increase in Ni extraction and a 10.16-point decrease in Fe dissolution. For the broader fraction, the corresponding observed changes were +8.52 points for Ni and −5.20 points for Fe. The Ni/Fe extraction ratio was approximately 2.47 and 1.92 times higher at 650 °C than at 550 °C for the fine and broader fractions, respectively. These differences describe the archived test outcomes and should not be interpreted as statistically resolved treatment effects.

The magnitude and direction of this response are consistent with the contemporary sulfation-roasting literature, which has repeatedly focused on maximizing Ni–Co dissolution

Nexus Science Review
INTERNATIONAL JOURNAL OF INTERDISCIPLINARY RESEARCH

Received: 01/08/2026 - **Accepted:** 13/09/2026
Vol: 01.04
DOI: 10.66104/ypw4n767
Pages: 1-45

while suppressing Fe transfer to solution (Mamyrbayeva et al., 2025; Osali et al., 2026; Ribeiro et al., 2020; Zhao, Li, Wang, & Xing, 2024). The present data add a practical size-fraction dimension to that selectivity problem.

3.5. Nickel extraction response

Nickel extraction increased monotonically across the three tested conditioning temperatures within each particle-size fraction. The highest observed value was 88.71% for the fine fraction at 650 °C. The broader fraction remained between 68.03 and 76.55% despite its higher head grade. Because conditions were not replicated, the monotonic pattern is reported descriptively, and no significance level or continuous temperature optimum is inferred.

Figure 6 shows the Ni response as a function of conditioning temperature for each fraction. Test 2 is annotated because its extraction calculation uses the nominal original ore mass.

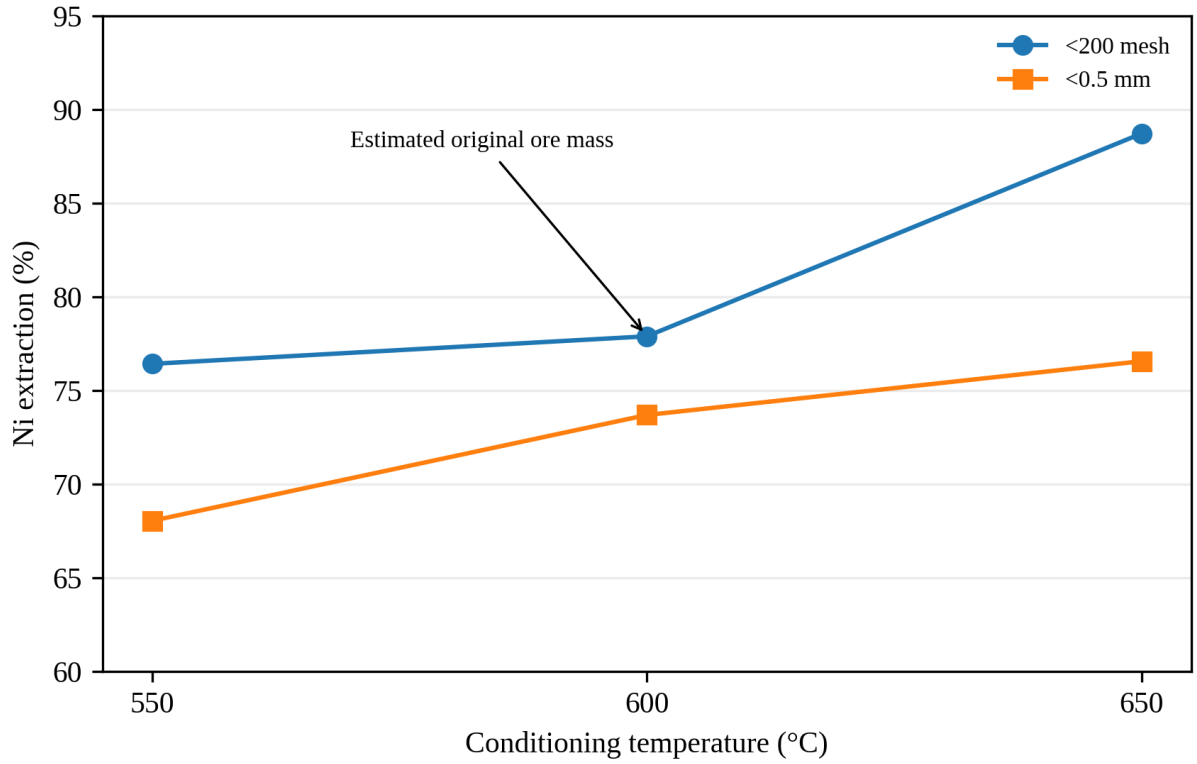

Nexus Science Review
INTERNATIONAL JOURNAL OF INTERDISCIPLINARY RESEARCH

Received: 01/08/2026 - **Accepted:** 13/09/2026
Vol: 01.04
DOI: 10.66104/ypw4n767
Pages: 1-45

Figure 6. Nickel extraction as a function of conditioning temperature for the two particle-size fractions. Test 2 is marked as estimated-basis because nominal original ore/reagent masses were used. [Evidence class: derived extraction calculations from archived analyses.]
Source: Authors' calculations from combined PLS and wash-liquor inventories.

The finer classified fraction showed the largest observed Ni response at 650 °C. Greater surface area and shorter diffusion length are plausible contributors, but they cannot be isolated from differences in feed composition, mineral-domain partitioning, and liberation created by classification. The result is therefore interpreted as a fraction-specific response rather than proof of a pure particle-size mechanism (Khan et al., 2026; Li, Liu, et al., 2026; Pereira, 2026).

3.6. Cobalt extraction response

Calculated Co extraction ranged from 81.41 to 93.96% across the six tests. Unlike Ni, Co did not show a fully monotonic temperature response in the broader fraction; its highest calculated extraction in that fraction occurred at 550 °C. However, Co mass-balance closure was systematically above 100%, reaching 115.14% in Test 8. At feed grades of only 0.099–0.115 wt.% Co, small absolute analytical deviations translate into relatively large percentage changes. Accordingly, the Co results support substantial recovery across the investigated window but not fine discrimination among nearby conditions.

Figure 7 presents Co extraction with the corresponding closure values shown as analytical-quality flags.

Nexus Science Review
INTERNATIONAL JOURNAL OF INTERDISCIPLINARY RESEARCH

Received: 01/08/2026 - **Accepted:** 13/09/2026
Vol: 01.04
DOI: 10.66104/ypw4n767
Pages: 1-45

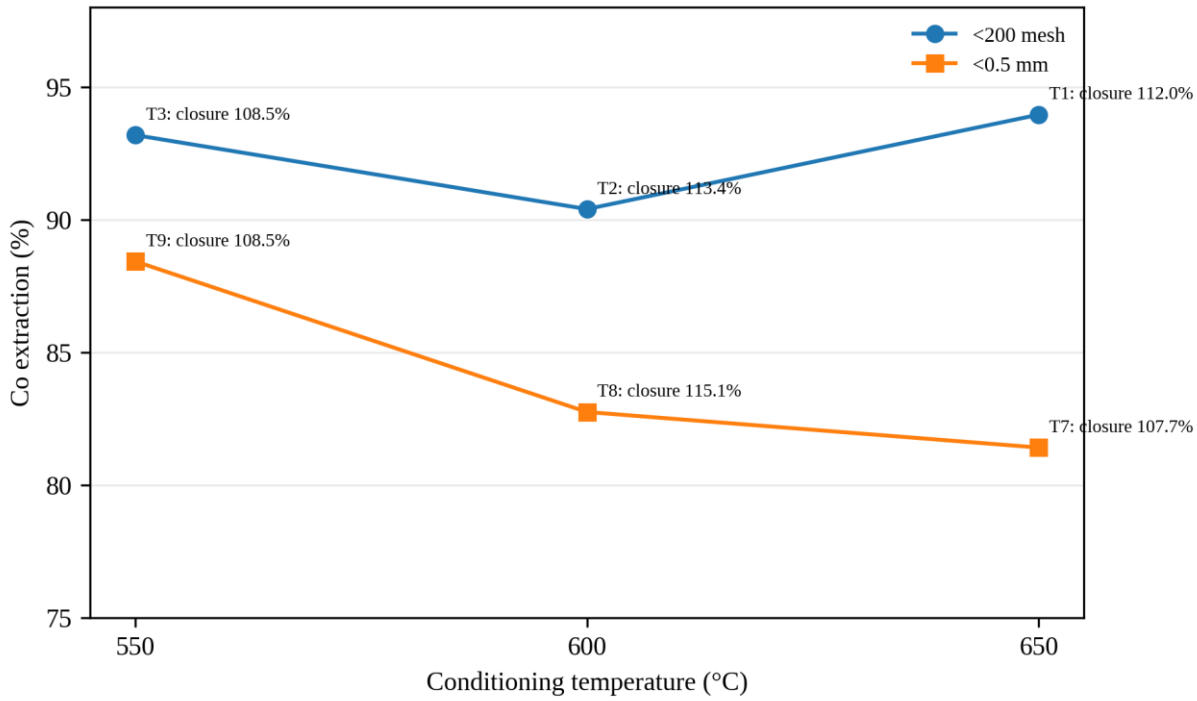

Figure 7. Cobalt extraction as a function of conditioning temperature, with Co mass-balance closure annotations. Test 2 is marked as estimated-basis because nominal original ore/reagent masses were used. [Evidence class: derived extraction calculations with analytical-quality flags.]
Source: Authors' calculations from archived analytical data.

The defensible conclusion is therefore that substantial Co recovery was calculated across the investigated window, whereas a precise temperature optimum cannot be established from the single-test dataset or the available analytical closure. This interpretation is consistent with the broader literature emphasis on simultaneous Ni–Co recovery from complex laterites and on process designs that preserve Co during selective Ni treatment (Acquah et al., 2026; Sun et al., 2026).

3.7. Iron dissolution and selectivity

Iron response provides the clearest descriptive trend associated with selective thermal conditioning. Fe dissolution was 9.03% and 7.36% at 650 °C for the fine and broader fractions, respectively, compared with 12.47–19.19% at lower tested temperatures. The observed decrease between 600 and 650 °C was approximately 8.4 percentage points for the fine fraction and 5.1 percentage points for the broader fraction. These values indicate improved Fe rejection at the highest tested temperature, but do not imply statistical significance.

Nexus Science Review
INTERNATIONAL JOURNAL OF INTERDISCIPLINARY RESEARCH

Received: 01/08/2026 - **Accepted:** 13/09/2026
Vol: 01.04
DOI: 10.66104/ypw4n767
Pages: 1-45

Figure 8 juxtaposes Fe dissolution with Ni/Fe selectivity, making the improvement at 650 °C explicit.

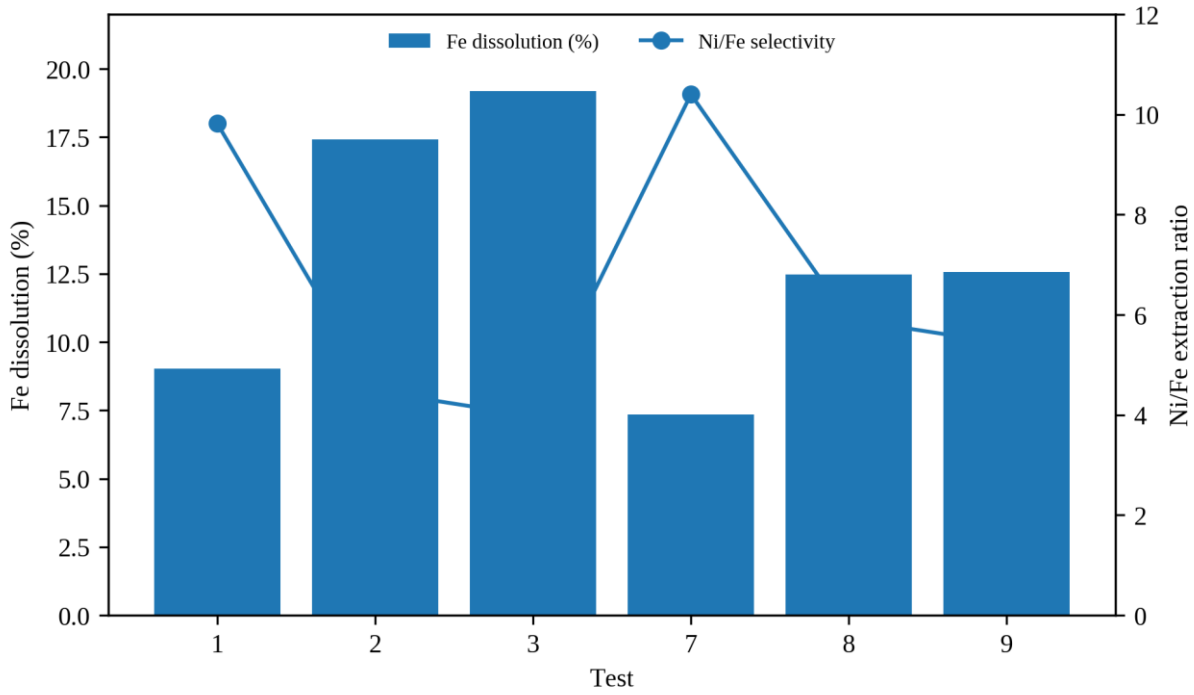

Figure 8. Iron dissolution and Ni/Fe selectivity for the six selective-sulfation tests. Test 2 is marked as estimated-basis because nominal original ore/reagent masses were used. [Evidence class: derived dissolution/selectivity calculations.]

Source: Authors' calculations from combined PLS and wash-liquor inventories.

The Fe trend is consistent with a working interpretation in which more soluble Fe-bearing sulfate or oxy-sulfate species persist at 550–600 °C, whereas a larger fraction of Fe reports to poorly soluble oxide-rich material at 650 °C. The complementary detection of $FeSO_4$ in a separate sulfation campaign supports the plausibility of residual Fe sulfate as a source of soluble Fe but does not directly identify the phase in the present calcines. From a flowsheet perspective, lower dissolved Fe would reduce subsequent neutralization and precipitation duty (Das & Li, 2023; Osali et al., 2026).

3.8. Dissolution of Al, Mg, Mn, Cr, and Zn

Minor-element behavior provides additional evidence about sulfur distribution and purification requirements. Table 7 reports solution-based extraction of Al, Mg, Mn, Cr, and Zn. Mn and Zn were strongly mobilized, Mg extraction remained near 45–50%, and Cr was

Nexus Science Review
INTERNATIONAL JOURNAL OF INTERDISCIPLINARY RESEARCH

Received: 01/08/2026 - **Accepted:** 13/09/2026
Vol: 01.04
DOI: 10.66104/ypw4n767
Pages: 1-45

largely refractory. Aluminum dissolution increased as conditioning temperature decreased, consistent with a larger residual inventory of soluble Al-bearing sulfate species at lower thermal severity.

Table 7. Solution-based extraction of selected gangue and minor elements. [Evidence class: derived extraction calculations from archived analyses.]

Test	Fraction	T (°C)	Al (%)	Mg (%)	Mn (%)	Cr (%)	Zn (%)
1	<200 mesh	650	42.69	48.19	88.20	2.60	69.57
2	<200 mesh	600	48.10*	45.26*	85.24*	4.72*	63.95*
3	<200 mesh	550	50.56	44.73	87.53	5.30	63.88
7	<0.5 mm	650	39.20	50.13	80.71	3.29	61.00
8	<0.5 mm	600	46.12	48.45	79.30	5.27	59.99
9	<0.5 mm	550	49.76	47.26	81.02	6.00	60.93

Source: Authors' calculations from archived PLS and wash-liquor analyses.
Note: *Test 2 values use the nominal 400 g ore mass.

The approximately 45–50% Mg extraction indicates substantial mobilization of Mg-bearing material. In the evaluated standard-state reaction set, $MgSO_4$ is a comparatively poor sulfate donor to NiO, so Mg-bearing sulfates may retain sulfate relative to the more favorable Fe(III)- and Al-sulfate transfer reactions. This does not establish $MgSO_4$ as an irreversible sink in the real multiphase ore. Literature on MgO/SiO_2 effects and sulfation–water leaching of Mg-rich nickel minerals likewise identifies Mg chemistry as a major determinant of acid and sulfur efficiency (Hariyanto et al., 2024; Yang et al., 2022). High Mn dissolution may also contribute to Co behavior if a fraction of Co is associated with Mn-bearing domains.

3.9. Particle-size-fraction effects

At equal nominal temperature, the <200 mesh fraction consistently produced higher percentage extraction of Ni and Co than the <0.5 mm fraction. At 650 °C, the difference was 12.16 percentage points for Ni and 12.55 points for Co; at 550 °C, the differences were 8.38 and 4.76 points, respectively. These contrasts are consistent with differences in interfacial access and diffusion length, but the two classified fractions also differed in the grades of Ni, Co, Fe, Mg, and Si. The results therefore demonstrate a fraction response, not an isolated grinding-size effect.

The broader fraction generally showed lower Fe dissolution despite its higher Fe grade. Restricted accessibility of reactive domains is one possible explanation, but compositional and

Nexus Science Review
INTERNATIONAL JOURNAL OF INTERDISCIPLINARY RESEARCH

Received: 01/08/2026 - **Accepted:** 13/09/2026
Vol: 01.04
DOI: 10.66104/ypw4n767
Pages: 1-45

mineralogical partitioning between size fractions is equally plausible. The process trade-off is therefore best expressed empirically as valuable-metal recovery versus impurity loading and downstream treatment duty, without assigning a unique particle-scale cause (Febriana et al., 2024; Pereira, 2026).

The higher head grade of the broader fraction partly offsets its lower percentage extraction. Test 7 recovered approximately 5.33 kg Ni/t ore and 0.94 kg Co/t, compared with 5.14 and 0.93 kg/t in Test 1. Test 7 therefore generated the highest prethermal process-value index despite its lower Ni extraction percentage. This result illustrates why process ranking based only on extraction percentage can be misleading.

3.10. Sulfate-transfer mechanism and thermodynamic interpretation

The combined evidence is thermodynamically consistent with a mixed sulfate-transfer working hypothesis. During the 250 °C stage, sulfuric acid can react with Fe oxyhydroxides and other reactive oxides to form sulfate-bearing species. During subsequent conditioning, Fe-bearing sulfates may decompose to Fe_2O_3 and sulfur oxides, while Ni- and Co-bearing sites made more accessible by host dehydroxylation may capture sulfate at solid–solid interfaces or through short-range SO_3 transport. The present dataset does not experimentally distinguish these pathways.

Table 8 summarizes selected reactions from the archived project thermodynamic dataset. Negative $\Delta G°$ and positive log K indicate thermodynamic favorability under the stated standard-state assumptions. Within this archived reaction set, ferric sulfate and aluminum sulfate are favorable sulfate donors to the NiO proxy; direct transfer from $MgSO_4$ or $FeSO_4$ to NiO with formation of MgO or FeO is unfavorable, whereas $FeSO_4$-mediated transfer becomes favorable when coupled to oxidation and Fe_2O_3 formation. NiO is used only as a thermodynamic comparison component and is not asserted to be a discrete phase identified in the ore. This pattern is conceptually consistent with prior thermodynamic work on iron(III)-sulfate-assisted laterite upgrading and experimental studies of low-temperature iron-oxide sulfation (Gontijo et al., 2020; Souza et al., 2022).

Nexus Science Review
INTERNATIONAL JOURNAL OF INTERDISCIPLINARY RESEARCH

Received: 01/08/2026 - **Accepted:** 13/09/2026
Vol: 01.04
DOI: 10.66104/ypw4n767
Pages: 1-45

Table 8. Archived standard-state sulfate-transfer thermodynamic data used for internal consistency screening. [Evidence class: archived thermodynamic plausibility dataset.]

Reaction	ΔG° (kcal) 550 °C	log K 550 °C	ΔG° (kcal) 600 °C	log K 600 °C	ΔG° (kcal) 650 °C	log K 650 °C
$3NiO + Fe_2(SO_4)_3 \rightarrow Fe_2O_3 + 3NiSO_4$	−28.134	7.470	−27.928	6.991	−27.754	6.571
$3NiFe_2O_4 + Fe_2(SO_4)_3 \rightarrow 4Fe_2O_3 + 3NiSO_4$	−15.455	4.104	−14.636	3.664	−13.797	3.267
$4NiO + 4FeSO_4 + O_2 \rightarrow 4NiSO_4 + 2Fe_2O_3$	−60.303	16.012	−57.279	14.338	−54.297	12.856
$FeSO_4 + NiO \rightarrow NiSO_4 + FeO$	+7.005	−1.860	+7.008	−1.754	+7.012	−1.660
$MgSO_4 + NiO \rightarrow MgO + NiSO_4$	+6.950	−1.845	+6.998	−1.752	+7.048	−1.669
$Al_2(SO_4)_3 + 3NiO \rightarrow Al_2O_3 + 3NiSO_4$	−24.512	6.508	−24.212	6.061	−23.910	5.661
$Fe_2(SO_4)_3 \rightarrow Fe_2O_3 + 3SO_3(g)$	+29.506	−7.835	+23.124	−5.788	+16.750	−3.966
$SO_3(g) + NiO \rightarrow NiSO_4$	−19.213	5.102	−17.018	4.260	−14.835	3.512

Source: Archived project thermodynamic reaction dataset; original software/database metadata were not preserved.

Note: ΔG° and log K values are retained from the archived dataset and were not independently regenerated. They are used only for standard-state consistency and plausibility screening, not as kinetic or phase-abundance evidence.

The overall ferric-sulfate transfer reaction can be expressed as the sum of ferric-sulfate decomposition and NiO sulfation by SO_3. Under the standard-state model, direct interfacial transfer and gas-mediated transfer yield the same overall products but operate at different mechanistic length scales. Thermodynamic equivalence does not establish which pathway occurred in the present furnace.

Table 9 presents the calculated SO_3 pressure window in which $Fe_2(SO_4)_3$ decomposition and NiO sulfation can occur simultaneously. The lower bound is the SO_3 pressure required to stabilize $NiSO_4$; the upper bound is the equilibrium pressure above which ferric sulfate decomposition is suppressed.

Table 9. SO_3 partial-pressure window calculated from the archived standard-state equilibrium constants. [Evidence class: derived thermodynamic plausibility calculation.]

Temperature	Minimum pSO_3 for NiO sulfation (bar)	Maximum pSO_3 for $Fe_2(SO_4)_3$ decomposition (bar)	Interpretation
550 °C	7.91×10^{-6}	2.45×10^{-3}	Broad thermodynamic window; generation rate may be kinetically limited

Nexus Science Review
INTERNATIONAL JOURNAL OF INTERDISCIPLINARY RESEARCH

Received: 01/08/2026 - **Accepted:** 13/09/2026
Vol: 01.04
DOI: 10.66104/ypw4n767
Pages: 1-45

600 °C	5.50×10^{-5}	1.18×10^{-2}	Greater Fe-sulfate decomposition and SO_3 availability
650 °C	3.07×10^{-4}	4.77×10^{-2}	Strongest SO_3 generation among tested temperatures while $NiSO_4$ remains stable

Source: Authors' calculations from the archived equilibrium constants. Note: The pressure window demonstrates standard-state plausibility only and does not reconstruct the unmeasured furnace-gas composition.

The calculated standard-state window shifts toward higher absolute pSO_3 as temperature increases. At 650 °C, the archived reaction set predicts a greater thermodynamic propensity for ferric sulfate decomposition while remaining within the pressure range in which $NiSO_4$ is stable. A static bed could develop local O_2 and SO_x gradients, but local gas composition was not measured; therefore, the pressure-window calculation is used only to demonstrate plausibility, not to reconstruct actual furnace gas conditions.

Recent studies that explicitly target SO_3 recovery, Na_2SO_4-mediated sulfur transfer, alkali-salt effects, and use of sulfate-bearing secondary streams support treating gas-solid sulfur transfer and sulfate recycling as central process variables (Candra et al., 2026; Hariyanto et al., 2023b; Zhao, Li, & Wang, 2025; Zhao et al., 2026). The present thermodynamic interpretation extends that concept to the observed Fe-rejection response.

Figure 9 integrates the measured metallurgical trends, complementary mineralogical context, and thermodynamic calculations into a working hypothesis. It explicitly separates direct observations from proposed host dehydroxylation, sulfate donation, gas-mediated transfer, sulfur retention/loss, and final Fe versus Ni–Co partitioning.

Nexus Science Review
INTERNATIONAL JOURNAL OF INTERDISCIPLINARY RESEARCH

Received: 01/08/2026 - **Accepted:** 13/09/2026
Vol: 01.04
DOI: 10.66104/ypw4n767
Pages: 1-45

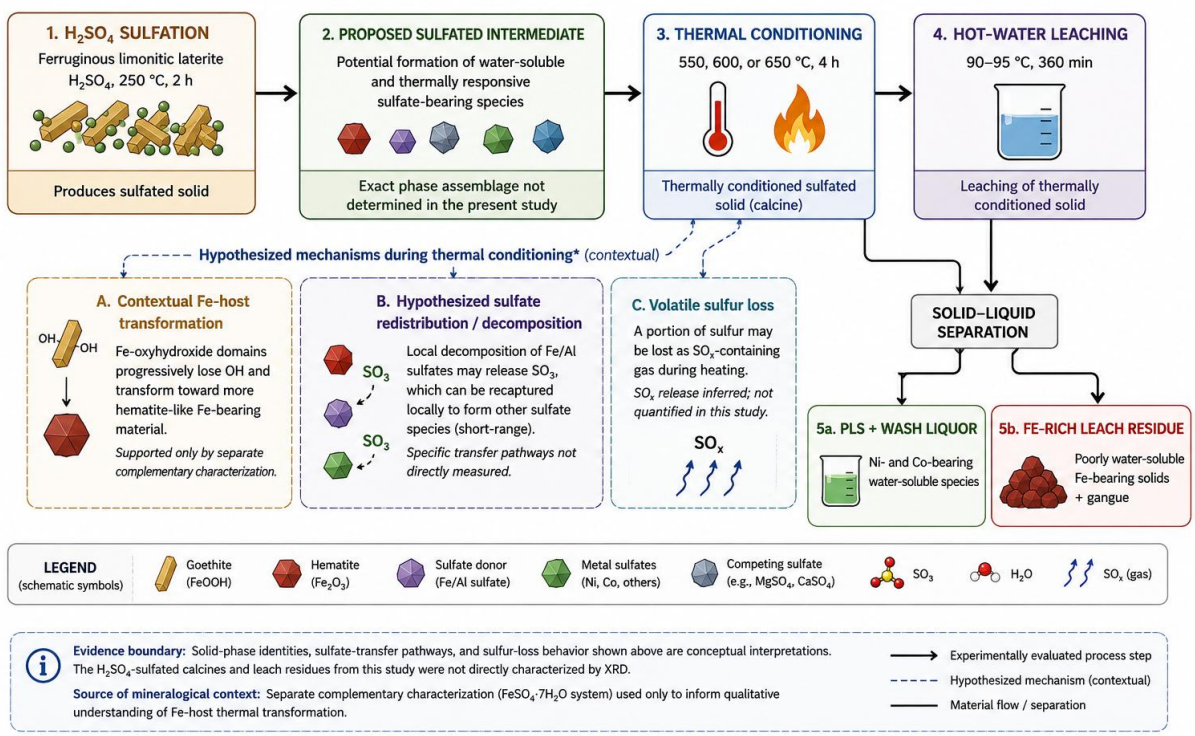

Figure 9. Working hypothesis for selective sulfate transfer and iron rejection during thermal conditioning and water leaching. [Evidence class: author-developed mechanistic working hypothesis.]
Source: Authors' mechanistic synthesis from the present experimental trends, complementary mineralogy, and thermodynamic calculations; conceptually informed by Gontijo et al. (2020), Souza et al. (2022), and Zhao et al. (2024–2026).

The mechanism in Figure 9 remains a working hypothesis rather than direct phase or gas-speciation proof. No direct XRD of the present calcines or residues, Fe oxidation-state spectroscopy, sulfur mapping, or simultaneous off-gas analysis is available. The figure is retained because it organizes the thermodynamic and complementary evidence, but all causal wording is restricted accordingly. Recent integrated flowsheets that combine sulfation roasting with selective leaching or precipitation illustrate the value of linking such mechanistic hypotheses to downstream separations (Zhao, Li, Wang, & Xing, 2025).

3.11. Mass-balance closure and filtration behavior

Table 10 reports mass-balance closure for the principal metals and the recorded filtration times. Ni and Fe closures were closer to unity than Co closures, although deviations remain material for an archived dataset. The systematically high Co closure reinforces the need

Nexus Science Review
INTERNATIONAL JOURNAL OF INTERDISCIPLINARY RESEARCH

Received: 01/08/2026 - **Accepted:** 13/09/2026
Vol: 01.04
DOI: 10.66104/ypw4n767
Pages: 1-45

for caution when interpreting relatively small differences among calculated Co extraction values.

Table 10. Metal-balance closure and filtration performance. [Evidence class: derived mass-balance closure plus direct archived filtration data.]

Test	Ni closure (%)	Co closure (%)	Fe closure (%)	PLS filtration	Wash filtration	Total filtration
1	110.86	112.00	101.56	3:20	2:04	5:24
2	105.61*	113.41*	100.33*	7:57	4:36	12:33
3	104.03	108.46	101.04	7:05	5:20	12:25
7	101.81	107.67	100.85	8:47	2:19	11:06
8	102.54	115.14	95.77	4:15	6:02	10:17
9	98.56	108.45	95.69	7:38	5:12	12:50

Source: Authors' calculations from solution inventories, dry-residue masses, and residue assays.
Note: *Test 2 closure uses nominal original ore mass.

The shortest total filtration time occurred in Test 1, which also combined the highest Ni extraction with low Fe dissolution. Tests 2, 3, and 9 required more than 12 min. Differences may reflect particle-size distribution, sulfate hydration, secondary precipitates, and cake structure, but the archived data do not contain filter area, pressure drop, cake thickness, or permeability. Accordingly, the filtration results are used only for comparative screening and not for scale-up.

Mass-balance closure is used here as a practical diagnostic of archived analytical uncertainty rather than as a formal measurement-uncertainty estimate. Across the six tests, Ni closure ranged from 98.56 to 110.86%, Co from 107.67 to 115.14%, and Fe from 95.69 to 101.56%. The systematic positive Co closure is particularly important because Co head grades were only 0.099–0.115 wt.%; small absolute analytical deviations therefore translate into large relative changes. These closure ranges define the level of caution required when comparing small differences among conditions.

3.12. Preliminary process-value and break-even screening

The process-value model is intentionally transparent and should be interpreted only as a comparative engineering-screening tool. Table 11 lists the illustrative coefficients used in the arithmetic. Recovered Ni and Co receive metal-value credits, while recorded acid-reagent addition, dissolved Fe, and six hours of leaching time receive simple penalties. These coefficients are not presented as current commodity forecasts, vendor quotations, or site-

Nexus Science Review
INTERNATIONAL JOURNAL OF INTERDISCIPLINARY RESEARCH

Received: 01/08/2026 - **Accepted:** 13/09/2026
Vol: 01.04
DOI: 10.66104/ypw4n767
Pages: 1-45

specific costs. The thermal stage is not charged in the prethermal index; instead, the difference between that index and the selected direct-leach screening benchmark is reported as a break-even allowance for otherwise unmeasured thermal and gas-treatment burdens.

Table 11. Assumptions used in the preliminary process-value screening. [Evidence class: author-defined illustrative screening assumptions.]

Parameter	Illustrative coefficient	Role in model
Ni value	US$16/kg Ni	Illustrative Ni metal-value credit
Co value	US$30/kg Co	Illustrative Co metal-value credit
Commercial H_2SO_4 addition cost	US$0.08/kg H_2SO_4 solution	Recorded reagent-solution penalty
Dissolved-Fe treatment penalty	US$0.03/kg Fe dissolved	Neutralization/purification proxy
Residence-time penalty	US$1.50/h/t ore	Residence-time proxy
Thermal energy, gas treatment, and CAPEX	Excluded from prethermal index	Evaluated only as break-even allowance

Source: Author-defined illustrative screening coefficients used solely for internal comparison; they are not current market forecasts or site-specific cost estimates.

Table 12 reports recovered metal masses, illustrative metal-value credits, operating proxies, and the prethermal process-value index. Test 7 ranked first because its higher feed grade compensated for the lower Ni extraction percentage; Test 1 ranked second and produced the strongest fine-fraction metallurgical response. The ranking is conditional on the stated coefficients and is not a profitability estimate. Calculated monetary values are retained to two decimal places only for arithmetic reproducibility, not as an indication of economic precision.

Table 12. Illustrative process-value screening results for the selective-sulfation tests. [Evidence class: derived engineering-screening calculations.]

Test	Ni (kg/t)	Co (kg/t)	Fe (kg/t)	Metal credit	Acid penalty	Fe penalty	Time penalty	PV index	Break-even allowance
1	5.14	0.93	20.23	110.12	16.50	0.61	9.00	84.01	51.61
2	4.51*	0.89*	39.04*	99.03	16.00	1.17	9.00	72.86	40.46
3	4.43	0.92	42.98	98.49	16.12	1.29	9.00	72.08	39.68
7	5.33	0.94	21.13	113.40	15.86	0.63	9.00	87.91	55.51
8	5.13	0.95	35.78	110.66	15.79	1.07	9.00	84.80	52.40
9	4.74	1.02	36.03	106.33	15.76	1.08	9.00	80.49	48.09

Source: Authors' calculations using the assumptions in Table 11.
Note: Monetary columns (metal credit, penalties, PV index, and break-even allowance) are US$/t ore. *Test 2 uses nominal original ore mass. "Break-even allowance" is the maximum combined thermal-energy, off-gas-treatment, thermal O&M, and annualized-capital burden that would reduce the condition to the US$32.40/t selected direct-leach screening benchmark under the illustrative assumptions.

Nexus Science Review
INTERNATIONAL JOURNAL OF INTERDISCIPLINARY RESEARCH

Received: 01/08/2026 - **Accepted:** 13/09/2026
Vol: 01.04
DOI: 10.66104/ypw4n767
Pages: 1-45

Across the six tests, the ratio of recorded commercial H_2SO_4-solution addition to recovered Ni plus Co was approximately 31.6–37.7 kg reagent solution per kilogram of recovered Ni+Co. Test 7 yielded the lowest value, consistent with its high recovered-metal mass and relatively low recorded reagent addition. This derived intensity is useful for internal comparison because it connects metallurgical response with reagent-solution use without implying an active-H_2SO_4 basis or full process cost.

The screening-value difference between 650 and 600 °C was fraction dependent. For the fine fraction, Test 1 exceeded Test 2 by approximately US$11.15/t before unmeasured thermal burdens. For the broader fraction, Test 7 exceeded Test 8 by only US$3.10/t. Under the illustrative coefficients, 600 °C could therefore rank above 650 °C for the broader fraction if combined savings in thermal energy, gas treatment, refractory, maintenance, and annualized capital exceeded approximately US$3.10/t ore. Because Test 2 uses nominal ore mass, the fine-fraction comparison is less certain and is treated only as indicative.

Because the process-value coefficients are author-defined screening assumptions, we added a one-at-a-time low/base/high sensitivity test to examine ranking dependence without presenting the bounds as forecasts or probability distributions. All non-varied coefficients were held at the Table 11 base case. The unmeasured thermal-stage burden is represented only as a uniform screening deduction because no condition-specific furnace-energy or gas-treatment data exist; a uniform deduction changes absolute indices but cannot by itself change the within-campaign rank order.

Table 13. One-at-a-time sensitivity of the illustrative process-value ranking to low/base/high assumptions. [Evidence class: derived engineering-screening sensitivity.]

Parameter varied	Low assumption	Base assumption	High assumption	Ranking outcome
Ni metal-value credit (US$/kg Ni)	12	16	20	7 > 8 > 1 > 9 > 2* > 3 at low/base/high
Co metal-value credit (US$/kg Co)	15	30	45	7 > 8 > 1 > 9 > 2* > 3 at low/base/high
Recorded commercial H_2SO_4-solution penalty (US$/kg solution)	0.04	0.08	0.16	7 > 8 > 1 > 9 > 2* > 3 at low/base/high
Dissolved-Fe treatment penalty (US$/kg Fe)	0.015	0.03	0.10	Low/base: 7 > 8 > 1 > 9 > 2* > 3; high: 7 > 1 > 8 > 9 > 2* > 3

Nexus Science Review
INTERNATIONAL JOURNAL OF INTERDISCIPLINARY RESEARCH

Received: 01/08/2026 - **Accepted:** 13/09/2026
Vol: 01.04
DOI: 10.66104/ypw4n767
Pages: 1-45

Parameter varied	Low assumption	Base assumption	High assumption	Ranking outcome
Uniform unmeasured thermal + off-gas + thermal O&M + annualized-capital burden (US$/t ore)	0	25	50	7 > 8 > 1 > 9 > 2* > 3; absolute index shifts equally

Source: Authors' calculations from the archived selective-sulfation dataset using deliberately broad illustrative bounds around the Table 11 base case. *Test 2 uses nominal original ore/reagent masses.
Note: These scenarios are one-at-a-time screening perturbations, not confidence intervals, commodity forecasts, vendor quotations, or site-specific costs. The top-ranked condition (Test 7) remains first in all tested perturbations. A high Fe-treatment penalty exchanges the second/third positions of Tests 1 and 8. A uniform thermal-stage deduction cannot change the ranking; only differential thermal burdens across temperatures can. On the existing base coefficients, the 600 °C broader-fraction condition would overtake its 650 °C counterpart if the combined unmeasured thermal-stage burden were more than approximately US$3.10/t ore lower. The analogous fine-fraction threshold is approximately US$11.15/t ore but is less certain because Test 2 is estimated-basis.

Figure 10 separates the base-case prethermal process-value index from the remaining unmeasured cost allowance assigned to the thermal stage. Together with Table 13, it emphasizes that the index is a bounded comparison tool rather than an economic valuation.

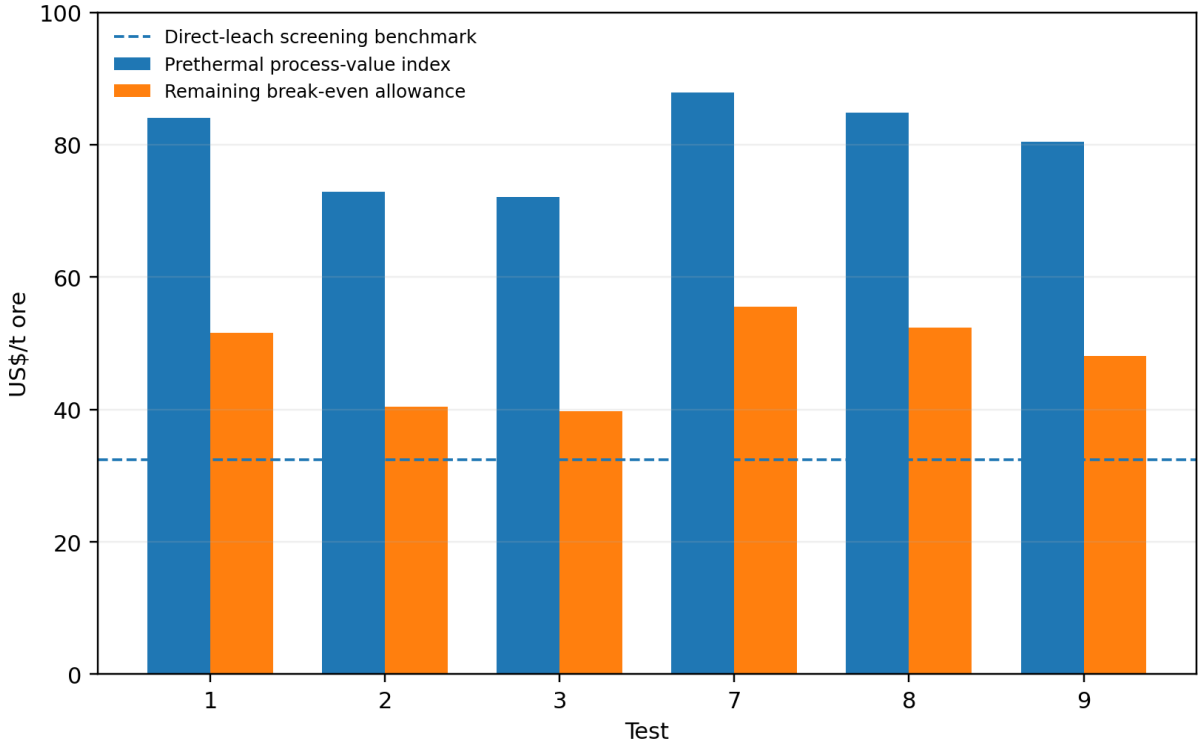

Figure 10. Prethermal process-value index and remaining combined thermal-energy, gas-treatment, thermal O&M, and annualized-capital break-even allowance for each selective-

Nexus Science Review
INTERNATIONAL JOURNAL OF INTERDISCIPLINARY RESEARCH

Received: 01/08/2026 - **Accepted:** 13/09/2026
Vol: 01.04
DOI: 10.66104/ypw4n767
Pages: 1-45

sulfation condition. Test 2 is marked as estimated-basis because nominal original ore/reagent masses were used. [Evidence class: derived engineering-screening visualization.]
Source: Authors' calculations using the base-case screening assumptions.

The approximately US$40–56/t break-even allowances do not demonstrate project viability. They define only a screening envelope within which the furnace, off-gas system, solids handling, maintenance, and annualized capital would have to operate to preserve the arithmetic difference relative to the selected direct-leach benchmark under the illustrative coefficients. No NPV, IRR, payability, downstream recovery, tax, site-specific energy price, or installed-cost model is implied (Chi et al., 2026; Sun et al., 2026; Zappala et al., 2024).

3.13. Comparison with direct atmospheric sulfuric-acid leaching

The separate direct-leaching dataset provides two contextual reference points: the condition with the maximum observed Ni extraction and the condition with the maximum base-case screening index. The benchmark reported 700–1000 kg H_2SO_4/t ore, whereas the selective-sulfation campaign used approximately 197–206 kg recorded commercial H_2SO_4 solution/t ore. Because the commercial-acid assay was not preserved and the benchmark values were recorded on a separate H_2SO_4 basis, these numbers are not normalized active-acid consumptions and their ratio must not be interpreted as a quantitative acid-saving factor. The feeds also differed, so the comparison illustrates process-intensity trade-offs rather than intrinsic route superiority.

Table 14 places the two 650 °C selective-sulfation conditions beside the two direct-leaching reference points. The ores, analytical programs, and archived acid-addition bases differed, so the comparison is indicative, non-causal, and unsuitable for statistical or normalized acid-consumption inference. Its purpose is to expose engineering trade-offs among recorded reagent addition, valuable-metal recovery, and Fe dissolution.

Table 14. Contextual comparison of selective sulfation with direct atmospheric leaching. [Evidence class: contextual benchmark using non-equivalent archived datasets.]

Route/ condition	Reagent (kg/t ore)	Leach time	Ni (%)	Co (%)	Fe (%)	Ni/Fe	PV index (US$/t)
Selective sulfation, Test 1 (<200 mesh, 650 °C)	206	360 min	88.71	93.96	9.03	9.82	84.01

Nexus Science Review
INTERNATIONAL JOURNAL OF INTERDISCIPLINARY RESEARCH

Received: 01/08/2026 - **Accepted:** 13/09/2026
Vol: 01.04
DOI: 10.66104/ypw4n767
Pages: 1-45

Selective sulfation, Test 7 (<0.5 mm, 650 °C)	198	360 min	76.55	81.41	7.36	10.40	87.91
Direct leach, best base-case economic scenario	700	420 min	66.2	41.4	42.9	1.54	32.40
Direct leach, maximum observed Ni extraction	1000	360 min	74.1	47.1	65.8	1.13	20.00

Source: Authors' calculations for the present selective-sulfation campaign and the Archived Atmospheric-Leaching Benchmark Dataset (n.d.).
Note: PV index = prethermal process-value index. Different ores, grades, mineralogy, experimental campaigns, and acid-addition bases were used. Selective-sulfation values are recorded commercial H_2SO_4-solution masses for which assay was not preserved; direct-leach values are the H_2SO_4 additions reported in the separate benchmark dataset. The values are not normalized to a common active-H_2SO_4 basis.

Figure 11 separates Ni extraction, Co extraction, Fe dissolution, and recorded acid-reagent addition into four panels. The figure is intended only as a contextual visual comparison; the ores and archived acid-addition bases differ.

Nexus Science Review
INTERNATIONAL JOURNAL OF INTERDISCIPLINARY RESEARCH

Received: 01/08/2026 - **Accepted:** 13/09/2026
Vol: 01.04
DOI: 10.66104/ypw4n767
Pages: 1-45

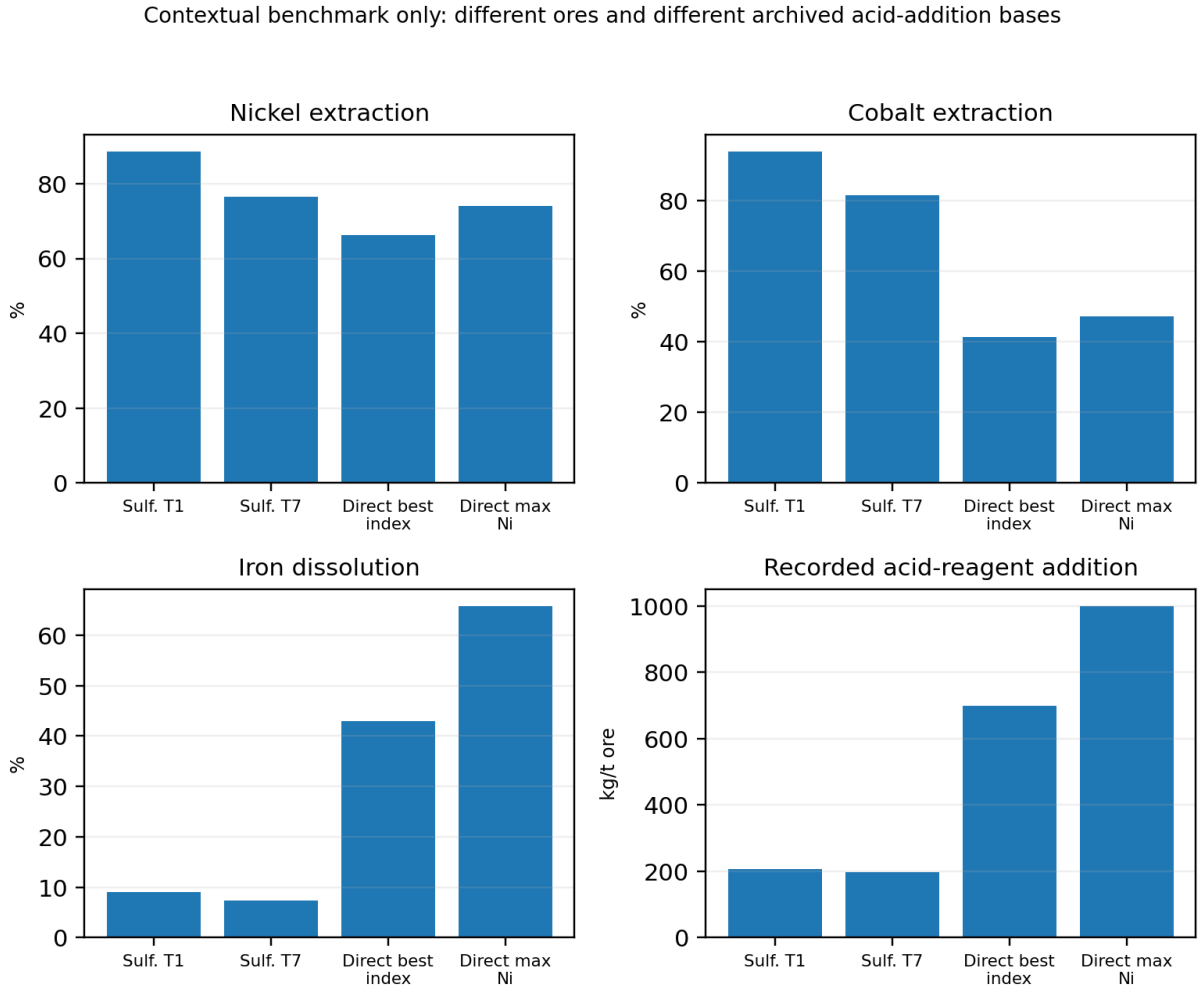

Figure 11. Contextual benchmark of Ni extraction, Co extraction, Fe dissolution, and recorded acid-reagent addition for selective sulfation and direct atmospheric leaching. [Evidence class: contextual benchmark.] Different ores, grades, mineralogy, experimental campaigns, and acid-addition bases were used; the reagent values are not normalized active-H_2SO_4 consumptions and must not be interpreted as an acid-saving factor or proof of route superiority. A valid route comparison requires a common feed, normalized active-acid basis, full energy balance, sulfur recovery, impurity purification, downstream Ni–Co recovery/payability, residue management, and capital intensity.

Source: Authors' compilation from the present archived sulfation campaign and the Archived Atmospheric-Leaching Benchmark Dataset (n.d.).

Within this contextual comparison, the selective-sulfation tests showed lower recorded reagent-addition numbers and lower Fe dissolution together with high Ni–Co recovery. Because both the ore and acid-addition basis differed, the magnitude of the reagent-addition contrast cannot be attributed solely to route chemistry or interpreted as a normalized active-acid saving. The direct process avoids the furnace and dedicated SO_x-control system, whereas

Nexus Science Review
INTERNATIONAL JOURNAL OF INTERDISCIPLINARY RESEARCH

Received: 01/08/2026 - **Accepted:** 13/09/2026
Vol: 01.04
DOI: 10.66104/ypw4n767
Pages: 1-45

selective sulfation transfers part of the process burden from solution-phase reagent and Fe treatment to thermal energy, sulfur management, off-gas treatment, and calcine handling. A defensible industrial comparison requires a common feed and a full flowsheet including active-acid basis, energy, sulfur recovery, impurity purification, residue management, product payability, and capital intensity (Acquah et al., 2026; Chi et al., 2026).

3.14. Technology maturity and scale-up requirements

The current dataset supports an early technology-opportunity assessment broadly analogous to front-end loading (FEL) 1 terminology and helps define the information required for later concept selection. The metallurgical response is sufficiently promising to warrant further engineering consideration, but the archived batch tests do not provide the energy, sulfur, gas, replicated performance, or continuous operability data needed for a bankable assessment. Table 15 distinguishes current evidence from the principal requirements for subsequent development.

Table 15. Technology maturity assessment and unresolved scale-up requirements for the selective sulfation route. [Evidence class: author-developed engineering-maturity synthesis.]

Workstream	Current evidence	Primary gap	Recommended FEL-equivalent stage
Metallurgical response	Ni, Co, Fe, pH, Eh, wash, residue, and filtration data available	Replicates and controlled pilot campaign	FEL 1 → FEL 2
Mineralogy	Complementary optical microscopy, XRD, and SEM–EDS evidence	Direct characterization of present calcines	FEL 2
Thermodynamics	Reaction feasibility and SO_3 pressure windows available	Kinetics and phase quantification	FEL 2
Energy	Thermal profile and residence time available	Measured kWh/t or fuel/t and heat recovery	FEL 2
Sulfur and emissions	Mass loss and visible fume observations	Complete S balance; SO_2, SO_3, acid mist, and dust measurements	FEL 2
Equipment concept	Muffle-furnace laboratory proof	Selection among rotary kiln, multiple hearth, fluidized bed, or zoned calciner	FEL 2
CAPEX/OPEX	Break-even thermal-cost allowance defined	Equipment sizing, quotations, maintenance, refractory, and gas-treatment costs	FEL 2–3

Nexus Science Review
INTERNATIONAL JOURNAL OF INTERDISCIPLINARY RESEARCH

Received: 01/08/2026 - **Accepted:** 13/09/2026
Vol: 01.04
DOI: 10.66104/ypw4n767
Pages: 1-45

Financial model	Comparative index available	Payability, downstream recovery, taxes, NPV, IRR, and sensitivity	FEL 3

Source: Authors' engineering-maturity interpretation based on the available evidence. FEL labels are used descriptively as front-end-loading shorthand and do not constitute formal project-gate certification.

Any future development campaign intended to move beyond screening should focus on the unresolved process variables that most directly control scale-up: conditioning temperature and time, controlled air flow and bed depth, measured furnace energy, sulfur balance, gas composition, calcine handling, dust generation, corrosion, and stability of Ni–Co extraction and Fe rejection under continuous or semicontinuous operation. The present manuscript does not claim that these data are available. Process-optimization studies such as Khan et al. (2026) illustrate the value of structured multivariable design once a credible operating window has been established.

Technology selection should also address how sulfur is supplied and recovered. Recent research on enhanced SO_3 recovery, Na_2SO_4-mediated sulfur transfer, and sulfate-bearing industrial secondary reagents suggests possible routes to lower fresh-acid demand or improve sulfur utilization, but these options require separate impurity, recycle, and emissions assessments before being transferred to the present ore system (Candra et al., 2026; Zhao, Li, & Wang, 2025; Zhao et al., 2026).

3.15. Sulfur balance as the critical missing scale-up variable

Sulfur redistribution is central to the proposed route but is not closed by the archived dataset. A defensible scale-up sulfur balance must quantify sulfur entering with the ore, recorded H_2SO_4 solution, and any sulfur-bearing redox reagent and reconcile it against sulfur retained in the calcine, leach residue, PLS, wash liquor, captured dust, and gas phase. The off-gas program must distinguish SO_2 and SO_3, quantify acid mist, dust loading, and water vapor, and report sulfur-capture/recovery efficiency. Without these measurements, productive sulfate transfer cannot be separated quantitatively from sulfur retained in non-productive gangue sulfates or lost to the gas train, and neither sulfur efficiency nor environmental burden can be established. This missing balance is therefore a primary gate between the present screening evidence and any claim of continuous-process viability.

Nexus Science Review
INTERNATIONAL JOURNAL OF INTERDISCIPLINARY RESEARCH

Received: 01/08/2026 - **Accepted:** 13/09/2026
Vol: 01.04
DOI: 10.66104/ypw4n767
Pages: 1-45

3.16. Study limitations, direct-characterization plan, and future experimental design

The principal limitation is the historical nature of the dataset. The six conditions were not replicated; the original sulfation mass record for Test 2 is missing; the commercial-acid assay was not preserved; the furnace gas atmosphere was neither controlled nor analyzed; and Co closure indicates material analytical uncertainty. The complementary mineralogical report used $FeSO_4 \cdot 7H_2O$ rather than H_2SO_4 and therefore supports interpretation only indirectly. No direct phase characterization of the present H_2SO_4-based calcines or residues, sulfate speciation, free-acidity measurement, sulfur balance, SO_2/SO_3/acid-mist/dust measurement, or furnace-energy measurement is available. The separate direct-leach dataset also uses a different ore and a non-demonstrably equivalent acid-addition basis. These limitations are treated as fixed boundaries of inference rather than as gaps filled by assumptions.

Accordingly, the manuscript restricts its conclusions to directly observed extraction, dissolution, mass balance, filtration, pH/Eh, and mass-loss trends; complementary mineralogical and thermodynamic analyses are used only to assess plausibility. Further process development would be most valuable where it adds replicated testing, direct calcine/residue characterization, a common active-acid basis, sulfur and energy balances, off-gas characterization, continuous-operability data, and downstream Ni–Co payability. Such measurements would connect the recorded reagent-solution response observed here to credible scale-up and sustainability assessment (Osali et al., 2026; Zhao, Li, Wang, & Xing, 2025; Zhao et al., 2026).

Table 16 converts the principal evidence gaps into a minimum next-step experimental program. The design is intentionally framed as a recommendation rather than as evidence generated by the present study.

Table 16. Recommended future experimental design and direct-characterization plan for advancing the selective-sulfation route. [Evidence class: author-developed future-work recommendation.]

Workstream	Required variables/measurements	Recommended next-step design objective
Replication and statistics	Independent replicate number; randomized test order; blanks/standards; full QA/QC	At least three independent replicates per selected condition before ANOVA, confidence intervals, response-surface modeling, or an optimization claim.

Nexus Science Review
INTERNATIONAL JOURNAL OF INTERDISCIPLINARY RESEARCH

Received: 01/08/2026 - **Accepted:** 13/09/2026
Vol: 01.04
DOI: 10.66104/ypw4n767
Pages: 1-45

Workstream	Required variables/measurements	Recommended next-step design objective
Thermal window	Conditioning temperature and time; heating rate; measured bed temperature	Expand beyond 550/600/650 °C and 4 h using a structured factorial or response-surface design after replication establishes repeatability.
Acid basis	Commercial-acid assay; solution mass; 100% H_2SO_4-equivalent dosage; free acidity	Normalize future comparisons on both recorded solution mass and independently measured active-H_2SO_4 basis.
Gas flow and bed geometry	Controlled air/O_2 flow; bed depth; superficial velocity; local gas sampling	Separate intrinsic chemistry from static-bed transport and quantify scale-sensitive gas–solid contact.
Particle-size distribution and feed	Narrow PSD fractions prepared from the same homogenized feed; complete chemistry/mineralogy by fraction	Isolate particle-size effects from grade and mineral-domain partitioning.
Redox during leaching	Reference electrode; temperature-corrected Eh/SHE basis; time-resolved pH/Eh; Fe^{2+}/Fe^{3+}; sulfite/sulfate species; reductant consumption	Treat redox as a measured, controlled variable rather than an archived final-state descriptor.
Calcine and residue characterization	XRD/Rietveld; SEM–EDS; EPMA; micro-XRF; XPS or Mössbauer/Fe speciation; sulfur mapping; soluble-sulfate analysis	Directly identify phase evolution, Fe oxidation state, Ni/Co host changes, sulfate distribution, and soluble versus refractory sulfur inventories.
Sulfur and off-gas balance	Total S in feed/reagents/calcine/residue/PLS/wash/dust/gas; SO_2; SO_3; acid mist; dust loading; water vapor; sulfur-recovery efficiency	Close the sulfur balance and quantify capture duty, emissions, and productive versus non-productive sulfur pathways.
Energy, operability, and downstream recovery	Measured kWh/t or fuel/t; heat recovery; corrosion/refractory wear; continuous/semi-continuous stability; Ni–Co purification/payability	Connect batch metallurgical response to equipment selection, OPEX/CAPEX, product recovery, and a later feasibility-level model.

Source: Authors' proposed development plan derived from the evidence gaps identified in the present retrospective screening study.

4. Conclusions

1. In the six archived single-test conditions, selective sulfation using approximately 197–206 kg of recorded commercial H_2SO_4 solution/t ore followed by hot-water leaching produced 68.0–88.7% Ni extraction, 81.4–94.0% calculated Co extraction, and 7.4–19.2% Fe dissolution. These values are descriptive; no statistical significance is claimed, and the commercial-acid assay was not preserved.

2. Among the tested temperatures, 650 °C gave the strongest observed Ni/Fe response within both particle-size fractions. The <200 mesh fraction gave the highest observed Ni extraction, whereas the <0.5 mm fraction gave the lowest Fe dissolution and the highest

Nexus Science Review
INTERNATIONAL JOURNAL OF INTERDISCIPLINARY RESEARCH

Received: 01/08/2026 - **Accepted:** 13/09/2026
Vol: 01.04
DOI: 10.66104/ypw4n767
Pages: 1-45

prethermal process-value index. Because classification also changed feed composition and the tests were not replicated, these are fraction-specific responses rather than isolated particle-size effects or statistical optima.

3. Complementary mineralogical observations from a separate $FeSO_4 \cdot 7H_2O$ campaign indicate a ferruginous Ni host and qualitative goethite-to-hematite transformation with heating, but they are not direct phase characterization of the present H_2SO_4-based calcines or residues. The observed temperature response is therefore described as consistent with, rather than proof of, progressive transformation or removal of soluble Fe-bearing sulfate species.

4. Archived standard-state thermodynamic data are consistent with a working hypothesis in which Fe(III)- and Al-bearing sulfates can act as sulfate donors, oxidation can make $FeSO_4$-mediated transfer favorable, $MgSO_4$ is a comparatively poor donor within the evaluated reaction set, and short-range SO_3 transfer is plausible. Because the original thermodynamic database metadata were not preserved, these calculations are used only as an internal consistency and plausibility screen and do not identify the dominant furnace mechanism.

5. Under the stated illustrative coefficients, the prethermal process-value indices were approximately US$72–88/t ore and the corresponding break-even allowances approximately US$40–56/t relative to the selected direct-leach screening benchmark. The sensitivity analysis shows that the within-campaign ranking is reasonably stable to broad one-at-a-time screening assumptions, but these values are not cash flow, NPV, IRR, profitability, or feasibility results. The direct-leach comparison is contextual and non-causal because the feeds and acid-addition bases differ; no environmental or economic superiority is inferred. A valid route comparison requires a common feed, measured active-acid basis, full energy and sulfur balances, SO_x/acid-mist/dust control, impurity purification, downstream Ni–Co recovery and payability, residue management, continuous operability, refractory/maintenance performance, and capital-intensity assessment.

Declarations

Funding

This study received no specific external funding.

Nexus Science Review
INTERNATIONAL JOURNAL OF INTERDISCIPLINARY RESEARCH

Received: 01/08/2026 - **Accepted:** 13/09/2026
Vol: 01.04
DOI: 10.66104/ypw4n767
Pages: 1-45

Conflict of Interest

The author declares no conflict of interest.

Data Availability

No new experiments were performed for this retrospective reanalysis. Quantitative results derive from the archived laboratory records and analytical certificates described in the manuscript. Supporting archived data may be made available subject to record availability and applicable confidentiality constraints.

Author Contributions

Withheld for double-blind review; the author-contribution statement will be restored after completion of blinded peer review.

References

Unpublished archival sources

Archived Atmospheric-Leaching Benchmark Dataset. (n.d.). Direct atmospheric sulfuric-acid leaching of a ferruginous nickel laterite [Unpublished laboratory dataset].

Archived Laboratory Campaign. (2011). Selective sulfation, thermal-conditioning, hot-water-leaching operating bulletins, and analytical certificates [Unpublished laboratory records].

Archived Mineralogical Characterization Report. (2009). Mineralogical characterization of a ferruginous nickel laterite before and after sulfation and dissolution [Unpublished technical report].

Peer-reviewed literature

Acquah, G., Skinner, W., Abaka-Wood, G., Spiridonov, P., Addai-Mensah, J., & Asamoah, R. (2026). Extraction of nickel and cobalt from complex low-grade lateritic ores: Challenges and opportunities. Minerals, 16(3), 287. https://doi.org/10.3390/min16030287

Candra, G., Yu, D., Liu, W., & Wang, Y. (2026). Industrial sodium sulfate wastewater as an alternative additive in sulfation roasting of laterite ore for selective metal recovery. JOM. Advance online publication. https://doi.org/10.1007/s11837-026-08601-1

Chi, D., Yu, J., Han, Y., Dong, Z., Gao, P., & Li, Y. (2026). Hydrometallurgical technologies of limonitic nickel laterite ore for carbon-neutral metallurgy: A review. JOM, 78(7), 6184–6210. https://doi.org/10.1007/s11837-026-08139-2

Crundwell, F. K., Moats, M. S., Ramachandran, V., Robinson, T. G., & Davenport, W. G. (2011). *Extractive metallurgy of nickel, cobalt and platinum group metals*. Elsevier. https://doi.org/10.1016/C2009-0-63541-8

Das, G. K., & Li, J. (2023). Iron removal as goethite from synthetic laterite leach solutions. ACS Omega, 8(13), 11931–11940. https://doi.org/10.1021/acsomega.2c07595

Febriana, E., Mulyadi, M. I., Mayangsari, W., Irawan, J., Setiawan, I., Maksum, A., Firdiyono, F., Oediyani, S., Prasetyo, A. B., & Soedarsono, J. W. (2024). Double-acting liberation of Ni and

Nexus Science Review
INTERNATIONAL JOURNAL OF INTERDISCIPLINARY RESEARCH

Received: 01/08/2026 - **Accepted:** 13/09/2026
Vol: 01.04
DOI: 10.66104/ypw4n767
Pages: 1-45

Co in the pre-treatment process to increase recovery of nickel from low-grade nickel laterite. Journal of Sustainable Mining, 23(3), 285–298. https://doi.org/10.46873/2300-3960.1422

Gao, J., Li, W., Ma, S., Du, Z., & Cheng, F. (2021). Spinel ferrite transformation for enhanced upgrading of nickel grade in laterite ore of various types. Minerals Engineering, 163, 106795. https://doi.org/10.1016/j.mineng.2021.106795

Gontijo, V. L., Teixeira, L. A. V., & Ciminelli, V. S. T. (2020). The reactivity of iron oxides and hydroxides during low-temperature sulfation. Hydrometallurgy, 197, 105452. https://doi.org/10.1016/j.hydromet.2020.105452

Hariyanto, R. K. S., Tomas da Rocha, L., Kim, S.-J., & Jung, S.-M. (2023a). Extraction behavior of nickel and cobalt from serpentine-rich ore through sulfation–roasting–leaching process. Metallurgical and Materials Transactions B, 54(6), 2915–2928. https://doi.org/10.1007/s11663-023-02934-x

Hariyanto, R. K. S., Tomas da Rocha, L., Kim, S.-J., & Jung, S.-M. (2023b). Influence of alkali salts on extraction of nickel from serpentine-rich ore through sulfation roasting leaching process. Journal of Sustainable Metallurgy, 9(4), 1636–1646. https://doi.org/10.1007/s40831-023-00753-7

Hariyanto, R. K. S., Tomas da Rocha, L., Cho, S.-K., & Jung, S.-M. (2024). Influence of SiO_2 and MgO on extraction of nickel and cobalt from laterite ores by sulfation roasting leaching process. Metallurgical and Materials Transactions B, 55(3), 1455–1470. https://doi.org/10.1007/s11663-024-03039-9

Khan, S., Bhargav, P. K., Chaudhuri, M. G., Majumder, A., & Dey, R. (2026). Process optimization for selective nickel recovery from limonite ore using the Taguchi method. Minerals Engineering, 247, 110511. https://doi.org/10.1016/j.mineng.2026.110511

Li, P., Zhu, X., Han, Y., & Li, W. (2023). Dehydroxylation of limonite ore for magnetization roasting: Phase transformation and kinetics analysis. Mining, Metallurgy & Exploration, 40(6), 2477–2486. https://doi.org/10.1007/s42461-023-00870-7

Li, Z.-X., Liu, Y.-L., Chang, J., Ju, X.-T., Huang, J., Li, J.-F., Zhang, J., & Yang, Z.-B. (2026). Sulfation roasting of the nickel laterite ore: Ammonia leaching kinetics study in selective Ni extraction. Canadian Metallurgical Quarterly, 65(2), 2021–2031. https://doi.org/10.1080/00084433.2025.2511508

Mamyrbayeva, K., Kuandykova, A., Chepushtanova, T., Merkibayev, Y., & Mishra, B. (2025). Investigation of the sulfation-roasting-water leaching process for efficient recovery of nickel and cobalt from Kazakhstan's laterite ore. Canadian Metallurgical Quarterly. Advance online publication. https://doi.org/10.1080/00084433.2025.2603070

McDonald, R. G., & Whittington, B. I. (2008). Atmospheric acid leaching of nickel laterites review: Part I. Sulphuric acid technologies. *Hydrometallurgy*, 91(1–4), 35–55. https://doi.org/10.1016/j.hydromet.2007.11.009

Osali, M., Ahani, F., Aboutalebi, M. R., Adeli, M., Moghaddam, J., Karimi, S., Wijenayake, J. J., & Alagha, L. (2026). Selective extraction of nickel and cobalt from limonitic laterite via optimized sulfation roasting–water leaching and solvent extraction. Minerals, 16(5), 431. https://doi.org/10.3390/min16050431

Pereira, A. C. (2025). Transformation of goethite into hematite: Mechanisms, technological routes, and industrial applications—A critical review (2020–2025). IKR Journal of Engineering and Technology, 1(2), 68–85. https://doi.org/10.5281/zenodo.17265013

Nexus Science Review
INTERNATIONAL JOURNAL OF INTERDISCIPLINARY RESEARCH

Received: 01/08/2026 - **Accepted:** 13/09/2026
Vol: 01.04
DOI: 10.66104/ypw4n767
Pages: 1-45

Pereira, A. C. (2026). From mineralogy to process design: The role of particle size distribution on nickel extraction kinetics and hydrometallurgical route selection in a limonitic laterite. IKR Journal of Engineering and Technology, 2(4). https://doi.org/10.5281/zenodo.21209619

Ribeiro, P. P. M., de Souza, L. C. M., Neumann, R., dos Santos, I. D., & Dutra, A. J. B. (2020). Nickel and cobalt losses from laterite ore after the sulfation-roasting-leaching processing. Journal of Materials Research and Technology, 9(6), 12404–12415. https://doi.org/10.1016/j.jmrt.2020.08.082

Ribeiro, P. P. M., dos Santos, I. D., Neumann, R., Fernandes, A., & Dutra, A. J. B. (2021). Roasting and leaching behavior of nickel laterite ore. Metallurgical and Materials Transactions B, 52(3), 1739–1754. https://doi.org/10.1007/s11663-021-02141-6

Souza, R. F. M., Tavares, M. A. A., Cruz, L. E. C., Oliveira, V. A. A., Santos, I. D., Moura, F. J., & Brocchi, E. A. (2022). On the cobalt content upgrade in nickeliferous laterites using iron (III) sulfate: A study based on thermodynamics simulations. Minerals, 12(9), 1156. https://doi.org/10.3390/min12091156

Sun, J., Wang, H., Zheng, X., & Sun, Z. (2026). A novel process for the treatment of low-grade laterite with the aim to a higher yield of valuable metals. Journal of Cleaner Production, 573, 148962. https://doi.org/10.1016/j.jclepro.2026.148962

Yang, X., Gao, L., Wu, Y., Chen, Y., & Tong, L. (2022). Extraction of magnesium and nickel from nickel-rich serpentine with sulfation roasting and water leaching. Metals, 12(2), 318. https://doi.org/10.3390/met12020318

Zappala, L., McDonald, R., & Pownceby, M. I. (2024). Nickel laterite beneficiation and potential for upgrading using high temperature methods: A review. Mineral Processing and Extractive Metallurgy Review, 45(7), 767–789. https://doi.org/10.1080/08827508.2023.2265533

Zhao, Z., Li, H., & Wang, C. (2025). An integrated sulfation-roasting-leaching process for coextraction of nickel and cobalt from laterite ores with enhanced SO_3 recovery. ACS Sustainable Resource Management, 2(1), 201–211. https://doi.org/10.1021/acssusresmgt.4c00437

Zhao, Z., Li, H., Wang, C., & Xing, P. (2024). Transformation mechanism and selective leaching of nickel and cobalt from limonitic laterite ore using sulfation-roasting-leaching process. Journal of Cleaner Production, 445, 141327. https://doi.org/10.1016/j.jclepro.2024.141327

Zhao, Z., Li, H., Wang, C., & Xing, P. (2025). Selective and efficient extraction of nickel and cobalt from laterite ores using the sulfation-roasting and leaching-precipitation process with H_2O_2 and surfactant addition. Hydrometallurgy, 237, 106546. https://doi.org/10.1016/j.hydromet.2025.106546

Zhao, Z., Wang, C., Li, G., Lu, D., Xing, P., & Li, H. (2026). Na_2SO_4-mediated sulfur transfer in co-extraction of limonitic and saprolitic laterites by sulfation-roasting-leaching. Minerals Engineering, 249, 110761. https://doi.org/10.1016/j.mineng.2026.110761